NASA TECHNICAL MEMORANDUM

NASA TM X- 72678

NASA TM X-72678

A STUDY OF REACTING FREE AND DUCTED HYDROGEN/AIR JETS

by H. Lee Beach, Jr.

NATIONAL AERONAUTICS AND SPACE ADMINISTRATION

LANGLEY RESEARCH CENTER, HAMPTON, VIRGINIA 23665

May 1975

45

NASA TECHNICAL MEMORANDUM

NASA TM X- 72678

NASA TM X-72678

A STUDY OF REACTING FREE AND DUCTED HYDROGEN/AIR JETS

by H. Lee Beach, Jr.

NATIONAL AERONAUTICS AND SPACE ADMINISTRATION

LANGLEY RESEARCH CENTER, HAMPTON, VIRGINIA 23665

May 1975

45

1. Report No.	2. Government Accession No.	3. Recipient's Catalog No.
NASA TM X-72678		

4. Title and Subtitle	5. Report Date
A STUDY OF REACTING FREE AND DUCTED HYDROGEN/AIR JETS	May 1975
	6. Performing Organization Code 37.430
7. Author(s)	8. Performing Organization Report No.
H. Lee Beach, Jr.	
9. Performing Organization Name and Address	10. Work Unit No.
NASA Langley Research Center Hampton, VA 23665	11. Contract or Grant No.
12. Sponsoring Agency Name and Address	13. Type of Report and Period Covered
National Aeronautics and Space Administration Washington, D.C. 20546	Technical Memorandum
	14. Sponsoring Agency Code

15. Supplementary Notes

Interim release of material to be combined with additional material and converted to a formal publication by December 1975.

16. Abstract

The mixing and reaction of a supersonic jet of hydrogen in coaxial free and ducted high temperature test gases were investigated. The focus of the study was to determine the importance of chemical kinetics on the computed results, and to test the ability of free-jet theoretical approaches to compute enclosed flow fields. Measured pitot pressure profiles were correlated by use of a parabolic mixing analysis employing an eddy viscosity model. All computations, including free, ducted, reacting, and nonreacting cases, used the same value of the empirical constant in the viscosity model. Equilibrium and finite rate chemistry models were utilized. The finite rate assumption allowed prediction of observed ignition delay, but the equilibrium model gave the best correlations downstream from the ignition location. Ducted calculations were made with finite rate chemistry; correlations were, in general, as good as the free-jet results until problems with the boundary conditions were encountered.

17. Key Words (Suggested by Author(s)) (STAR category underlined)	18. Distribution Statement
Aircraft Propulsion and Power Fluid Mechanics and Heat Transfer Aerodynamics	Unclassified - Unlimited

19. Security Classif. (of this report)	20. Security Classif. (of this page)	21. No. of Pages	22. Price*
Unclassified	Unclassified	44	

*Available from { The National Technical Information Service, Springfield, Virginia 22151
STIF/NASA Scientific and Technical Information Facility, P.O. Box 33, College Park, MD 20740

A STUDY OF REACTING FREE AND DUCTED HYDROGEN/AIR JETS

By H. Lee Beach, Jr.
Langley Research Center

SUMMARY

The mixing and reaction of a supersonic jet of hydrogen in coaxial free and ducted high temperature test gases were investigated. The focus of the study was to determine the importance of chemical kinetics on the computed results, and to test the ability of free-jet theoretical approaches to compute enclosed flow fields. Measured pitot pressure profiles were correlated by use of a parabolic mixing analysis employing an eddy viscosity model. All computations, including free, ducted, reacting and nonreacting cases, used the same value of the empirical constant in the viscosity model. Equilibrium and finite rate chemistry models were utilized. The finite rate assumption allowed prediction of observed ignition delay, but the equilibrium model gave the best correlations downstream from the ignition location. Ducted calculations were made with finite rate chemistry; correlations were, in general, as good as the free-jet results until problems with the boundary conditions were encountered.

INTRODUCTION

Interest in hypersonic air-breathing engines during the past several years has led to a number of investigations into technology areas contributing to supersonic combustion ramjet (scramjet) engine design. Papers such as references 1 to 4 give an account of the technology status of current scramjet concepts. Reference 5 points out that an extremely desirable feature of the new concepts utilizing hydrogen fuel is that engine cooling requirements involve only a portion of the total fuel heat sink, and the remaining fuel is then available for cooling the vehicle structure. The design of such an engine demands the ability to accurately predict the distribution as well as amount of heat release in the combustor in order that cooling requirements are not achieved at the expense of performance. A primary problem area is therefore the flow field description downstream of a fuel injector (ref. 6).

This is, of course, but one example in a broad class of problems concerning free turbulent mixing - an area which has received a great deal of recent attention. It has become quite apparent that the trends in analysis are going far beyond traditional mixing length and eddy viscosity modeling, to additional partial differential equations describing turbulence quantities, and even to statistical formulations. The trends can be followed in reference 7, which summarizes data and theory through early 1970; reference 8, which

summarizes the attempts of many qualified researchers to analyze the same nonreacting test cases with their own solution techniques; and reference 9, which adds to reference 8 the most recent views, particularly regarding reacting flows and statistical approaches.

Although significant progress seems to have been made in computationally describing the physics of turbulent mixing flow fields, it remains true that for many practical research and design situations, sufficient confidence in the new techniques has not yet been achieved. In these instances, older approaches must be utilized. (See discussion in ref. 10.) Reference 11, for example, discusses an extension of stirred reactor theory applicable to gas turbine combustors, and reference 12 describes a variety of approaches to problems pertinent to scramjet engine flow fields.

Over a period of years there have been a number of investigations at NASA Langley Research Center designed specifically to provide heterogeneous mixing results from which scramjet engine design and performance calculations could be made. These have included tests with parallel injectors (refs. 12-15), perpendicular injectors (refs. 16 and 17), and several injection angles in between (ref. 18). The nonparallel injection cases have traditionally been handled with one-dimensional analyses due to the very complex flow field behavior at the injection ports. Good success in correlating free parallel mixing data has been achieved, however, with boundary-layer-type analyses with turbulence introduced through an eddy viscosity model and turbulent Prandtl and Lewis numbers. The viscosity model which has been developed (ref. 14) for nonreactive mixing accounts for density variation, a necessity also indicated by references 7 and 19.

Underlying the work on viscosity model development has been the hope that mixing rates will be the same with and without reaction, or at least that the same modeling can be utilized for both. Reference 6 indicated that the latter is the case; that is, the eddy viscosity model has enough flexibility built in to account for the large differences in reacting and non-reacting flows without changing the empirical constant. This was determined by comparing experimental pitot profiles and the predictions thereof for two high temperature flows which were the same except one utilized nitrogen to simulate air and was therefore nonreacting. Reacting calculations were performed with an equilibrium chemistry model which ignored an observed ignition delay distance, so the possible effect of chemical kinetics was not determined.

Another important consideration in the computation of flows for engine application is that of flow boundaries. Since the turbulent mixing regions in the engines are enclosed, the ability of the models under development to handle ducted flow fields in a reasonable way must be determined. Some pessimism in this area has already been indicated in references 20 and 21.

The purpose of this report is to extend the results of reference 6 to consider kinetics effects, and to compute the ducted coaxial flow of reference 6 with the same parabolic theory which is used for free-jet flows. The test conditions involve five cases of supersonic (M=2) injection of hydrogen into supersonic (M=2) jets of:

Case	Test Gas	Test Gas T_t	H_2 T_t	Geometry
1	Air	2220 K	450 K	Free Jet
2	N_2	2220 K	450 K	Free Jet
3	Air	1800 K	350 K	Free Jet
4	Air	2220 K	450 K	Ducted
5	N_2	2220 K	450 K	Ducted

Evaluations are made by comparing theoretical and experimental values of pitot pressure. Since this is not a conventional quantity used in mixing and reacting theory evaluation, its sensitivity for such use is discussed.

SYMBOLS

D_j	hydrogen injector outside diameter
k	empirical constant in viscosity model
P	heater stagnation pressure
P_{t_2}	pitot pressure
R	radial distance measured from flow centerline
T	static temperature
T_t	stagnation temperature
U	velocity
U'	velocity defined by equation (2)
U''	velocity defined by equation (3)
X	axial distance measured from injector exit
z	mixing zone width in viscosity model
α_{H_2}	mass fraction of unreacted hydrogen
α_{H_2O}	mass fraction of water
ε_t	kinematic viscosity

η_c combustion efficiency

η_m mixing efficiency

Subscripts:

a conditions in freestream

$_{C_L}$ conditions at centerline

APPARATUS AND PROCEDURE

The apparatus and procedure were described in reference 6, but the description is repeated here for clarity. The experimental program was conducted at the Langley Ceramic Heater (ref. 22) which provided the high temperature test gas. The heater is the storage type with a bed of zirconia and alumina pebbles; it is capable of producing stagnation temperatures to 2220 K and stagnation pressures to 5.5×10^6 N/m^2 for either air or nitrogen. Test gas total temperatures were inferred from extensive measurements reported in reference 23, which correlate the temperature of the pebble bed with gas total temperature.

A schematic of the experimental apparatus is shown in figure 1. The test gas nozzle was a Mach 2 (nominal), axisymmetric, stainless steel design cooled by approximately 5.7 kg/sec of water. Nozzle coordinates were scaled from reference 24 to give an exit diameter of 6.53 cm which was judged to be the maximum diameter for Mach 2 yielding acceptably low dust levels from the heater. A stagnation pressure of approximately seven atmospheres was required to produce a nozzle exit static pressure of one atmosphere, and the corresponding test gas flow rates were 1.15 kg/sec and 1.28 kg/sec for the high and low temperature cases, respectively.

The hydrogen injector mounted on the nozzle centerline was a 0.95 cm stainless steel tube with a Mach 2 nozzle inserted at the exit. The resulting injector lip thickness was approximately 1.5 mm. During tests the centerbody was cooled by the injectant which originated from an ambient temperature supply. Hydrogen stagnation pressure was adjusted to give a one-atmosphere (matched) exit static pressure. Calculated temperature rises of the hydrogen passing through the injector were 150 K and 53 K for the high and low temperature cases, and the resulting flow rates of 7.7 g/sec and 8.2 g/sec yielded overall equivalence ratios of 0.225 and 0.23.

To provide a means of making enclosed as well as free-jet measurements, constant-area ducts 30.5 cm and 45.7 cm in length were attached to the nozzle. The ducts were constructed of stainless steel, uncooled, and contained numerous static pressure ports and embedded thermocouples along the duct axially and around the circumference.

In-stream measurement for the experiments consisted of pitot-pressure profiles at various axial locations. The probe was a modified version of that described in reference 25, and had an outside diameter of 6.3 mm with a tip half-angle of 30°. It was used in a continuous traverse mode driven at a rate of approximately 5 mm/sec perpendicular to the main flow direction. Records of pitot pressure versus transverse position were obtained on an oscillograph recorder. Frequent checks of pitot pressure at a given point with the probe moving and stationary indicated that resolution for the moving probe was fast enough for accurate measurement.

Photographic records of the flow field have proved beneficial in interpreting and analyzing results. Sixteen mm color movies taken at a speed of 24 frames/sec and photographs taken with a 70 mm camera give good representation of the reacting flows, and they have been used to estimate emission delay as well as the spread of the mixing-reacting region. Shadowgraphs have also been useful, particularly in the interpretation of near-field phenomena for both reacting and nonreacting flows.

RESULTS AND DISCUSSION

Photographs

Examples of typical Case 1 and Case 3 flow fields are shown in the photographs of figure 2. The nozzle exit and injector lip are both visible. There is a definite separation of the flame from the injector lip in each case, although the separation distance appears to be shorter and more clearly defined for Case 1. Also apparent is a spread of the flame boundary in the downstream direction. Both emission delay and flame spread were expected qualitative observations, but quantitatively they were found to vary somewhat with film exposure. The emission delay lengths of approximately 2.5 injector diameters and 6.5 injector diameters shown in figure 2 are therefore only approximations to the actual ignition delay length. For example, photographs and 16 mm movies of the low temperature tests have indicated emission delays ranging from 4.5 to 7.5 injector diameters.

Shadowgraphs illustrating the aerodynamic features of the near field in the reacting and nonreacting flows are shown in figure 3 (from reference 6). An expansion at the nozzle exit, an expansion and re-compression shock associated with the main flow at the relatively thick injector lip, and a conical shock in the hydrogen jet which converges at approximately 1.3 diameters and penetrates into the main flow are all visible. A distinct change in wave angle is evident as the latter shock crosses the hydrogen/air interface. This is indicative of the Mach number gradient caused by the wake-like region behind the lip and local effects of mixing and reaction. Note that the width of the mixing region at a given axial location appears greater for the reacting case due to combustion-induced streamline divergence.

It is significant that the wave patterns for the various cases are similar. The waves are relatively weak, on the order of 6° turning based

on calculations from pitot pressure measurements. They are therefore neglected in the analysis even though pressure gradients certainly exist both radially and axially, particularly in the near field (less than six injector diameters).

Theoretical Method

A discussion of the basic theoretical approach is given in reference 26. The analysis utilizes laminar boundary-layer equations and a Von Mises transformation; turbulence is introduced through the eddy viscosity and turbulent Prandtl and Lewis numbers. The viscosity model is described in reference 13 where the kinematic viscosity is defined as

$$\varepsilon_t = k\ z\ U_{C_L}\ ; \tag{1}$$

k is an empirical constant and U_{C_L} is the centerline velocity. The quantity z is the mixing zone width defined as the radial distance between points where the local velocities U' and U'' are

$$U' = U_a + 0.95\ (U_{C_L} - U_a) \tag{2}$$

and

$$U'' = U_a + 0.5\ (U_{C_L} - U_a) \tag{3}$$

The velocity U_a is the constant free-stream test gas velocity for the unconfined flows, and is the peak test gas velocity (changing with axial distance) for the ducted flows. Local values of turbulent (eddy) viscosity are found by multiplying ε_t by the local density.

Input requirements for the computer program (ref. 27) include initial radial distributions of velocity, static temperature, and composition. Due to the boundary layer on the injector and the rather thick injector lip, it was judged that step profiles in velocity and temperature would not suffice. Instead, a Mach number profile was generated from the nozzle-exit pitot distribution shown in figure 4 and the assumption of uniform static pressure; temperature and velocity profiles were calculated from this distribution by assuming a total temperature profile and a step change in composition at the mid-point of the injector wall. Additional specifications of wall friction coefficient and wall temperature were required for the ducted flows.

Both equilibrium and finite rate chemistry models were employed. The latter is described in references 28 and 29, and adds the capability of accounting for chemical kinetic effects including ignition delay. This often requires, however, significant tampering with the initial profiles since ignition is quite sensitive to initial temperature and concentration (if free radicals are present). To examine this sensitivity, four different total temperature profiles were assumed for Cases 1 and 3, yielding four sets of input temperature and velocity profiles. The assumptions are illustrated in figure 5. The first is simply a step change in T_t from the bulk hydrogen to the bulk free-stream value at the mid-point of the injector wall. The

second is a linear change in T_t through the injector wall. The third is also a linear change in T_t, but spans the entire boundary-layer/wake region shown in the exit pitot pressure profile in figure 4. The fourth involves calculations of injector wall temperature and different linear changes in T_t through the boundary layers and the wall. Predicted ignition delay distances for both high and low temperature cases are also shown in figure 5. Ignition was judged to begin at the axial location where a water mass fraction of 1 percent was produced somewhere in the profile. For several cases ignition did not occur in the ten injector diameter distance computed, and a wide range of delay distances was found. The assumption of a linear T_t change through the injector wall resulted in a Case 1 ignition delay distance corresponding very closely to the observed emission delay of figure 2; the corresponding assumption for Case 3 also yielded a reasonable approximation to observed emission delay. Based on this result, all subsequent analysis has been performed with the assumption of a linear change in T_t through the injector wall.

Free-Jet Results

All free-jet computations were made using the same viscosity model (described previously) and the same value of the empirical constant (0.01). Turbulent Prandtl and Lewis numbers were 0.9 and 1.0, respectively. Results for centerline pitot pressure decay with axial distance are presented in figures 6(a), 6(b), and 6(c) corresponding to Cases 1-3, respectively. Note that 1 and 2 provide the same test condition for reacting and nonreacting flow, and that good agreement between data and theory is apparent for both cases. Little difference is seen between the equilibrium and finite rate calculations. For Case 3, neither the equilibrium nor the finite rate calculations agree well with the near-field data points. Beyond 6.5 injector diameters (the approximate ignition point), the curves separate; at the downstream data points the equilibrium calculation agrees well, but the finite rate calculation is significantly worse. The third curve in figure 6(c) was generated by using the finite rate model until the reaction started ($0 < X/D_j \leq 6.5$) and the equilibrium model thereafter ($X/D_j > 6.5$). This combined calculation predicts a centerline decay very nearly the same as the equilibrium calculation. It appears from figure 6(c) that the finite rate chemistry model and/or the turbulence model are inadequate for handling the low-temperature case.

Perhaps a better test of the theory is afforded by examination of theoretical and experimental radial profiles of pitot pressure. Figures 7(a) through 7(c) give profile results at axial stations of 6.7, 18.7, and 26.7 jet diameters for Cases 1, 2, and 3. The theory predicts the minimum pitot pressure and the spread of the mixing region relatively well for Cases 1 and 2, and the theoretical profiles of the equilibrium and finite rate models are very similar. The implication is that chemical kinetics is not important for the high temperature condition, but this will be discussed in later sections. Comparing Cases 1 and 2, the anticipated effects of heat release are apparent. Combustion-induced streamline divergence is evidenced by the greater spread of the mixing region for Case 1. Also, lower Mach numbers caused by the reaction are implied by the pitot pressures throughout

the mixing region; this is inferred since relative levels of pitot pressure correspond roughly to relative levels of Mach number. The close agreement of the equilibrium and finite rate high temperature calculations provides little opportunity for evaluation of the comparative merits of the chemistry models.

The low temperature Case 3, as seen in figure 7(c), has interesting features from the kinetics point of view. At the 6.7 diameter station, predicted centerline pitot pressures are the same, but the finite rate calculation gives a much better representation of the profile. This is reasonable since the reaction has just begun at about this station, and a serious overprediction of combustion-induced Mach number and streamline effects would naturally result by assuming the reaction started at $X/D_j = 0$. At the downstream locations, the equilibrium calculation appears to give better results than the finite rate, particularly near the center of the flow. Based on these pitot pressure comparison, then, the best model for the chemistry utilizes finite rate to predict ignition delay and equilibrium thereafter.

An important point to be made in conjunction with the free-jet pitot pressure correlations is: since all computations were made using the same viscosity model and the same value of the empirical constant, it therefore appears that enough flexibility is built into the viscosity model to account for the large density and composition differences in reacting and nonreacting flows (as also reported in reference 6).

Ducted Results

Enclosing the mixing/reacting flow introduces a number of problems both in data interpretation and in theoretical modeling. Discrete waves, which appear to be attenuated rather rapidly in the free flows, reflect and re-intersect the mixing region for ducted flows. The parabolic analysis used in this report is not capable of treating these discrete waves. Computation time is greatly increased over the free flows by the fact that an extra iteration loop is needed for the pressure; also grid points far beyond the edge of mixing must be carried in order to introduce the effects of the boundaries on the solution. The boundary conditions are not handled rigorously, and therefore true boundary layer thicknesses are not computed.

Static pressure distributions on the duct walls for Cases 4 and 5 are shown in figures 8(a) to 8(c). Results for both the 30.5 cm duct and the 45.7 cm duct are presented for Case 4. The effects of the waves are obvious for both the reacting and nonreacting data, but the trend of these data clearly shows the increased pressure rise from combustion. Predictions of static pressure using the parabolic analysis are also shown on the figures. Reasonable data trends are produced for Case 5 and Case 4 up $X/D_j \cong 35$.

Beyond $X/D_j \cong 35$, difficulties in the computation were encountered. A combination of circumstances related to the viscosity model, boundary conditions, and the basic coordinate system (using stream function) led to these difficulties. The solid curve on figure 8(b) was obtained by the original analytical approach mentioned previously. The sharp change in slope was

initiated when the viscosity model became unstable; this occurred when U' and U'' reached nearly the same magnitude and the mixing width z was unreliable. The dashed curve shows the effect of bounding the mixing zone width; the calculation proceeded further, but stopped at $X/D_j \cong 42$.

Both of these computations ceased when the computer program, operating with equal increments in the stream function, could not cope with the low velocities and temperatures close to the wall. It appears that this difficulty is inherent to the particular computer program used, and would eventually occur for any ducted flow computation using this program. In order to obtain theoretical pitot pressure profiles to compare with those measured at the exit of the 45.7 cm duct, a linearly varying pressure as shown in figure 8(b) in the region $32 < X/D_j < 48$ was assumed; the calculation was then performed without accounting for boundary effects.

Experimental and theoretical duct-exit pitot profiles are presented in figure 9. In view of the shocks, expansions, and computational problems, surprisingly good data/theory agreement is found in the mixing and reacting zones. The discrepancies outside the mixing region can perhaps be explained (in addition to neglect of waves) by the probability that the wall boundary layer and mixing layer have merged in the real case but not in the theoretical case. The good agreement, particularly for the 30.5 cm duct in Case 4, is encouraging. Still, the basic computation approach, involving equal increments in the stream function, is not satisfactory. It would be an improvement to utilize a dimensionless stream function defined in terms of local and bounding values of stream function as described in reference 30.

Pressure Sensitivity

Evaluation of theoretical mixing models usually involves data/theory comparisons of velocity and species concentration, and temperature comparisons are highly desirable. In this report, comparisons of pitot pressure only are made. Since pitot pressure depends on all of the above-mentioned variables, a question concerning the sensitivity of the pitot pressure results relative to the other variables naturally occurs.

Figures 6(a) and 7(a) showing Case 1 pitot pressure calculations indicate very nearly the same pitot pressures for the equilibrium and finite rate chemistry models. Figures 6(c) and 7(c) for Case 3 also show two calculations yielding very similar pitot pressures for the downstream profiles. One way to approach the sensitivity question is to examine the other calculated variables for Cases 1 and 3 and see if they compare as well as the pressures.

Centerline decays of velocity and unreacted hydrogen mass fraction are shown for Case 1 in figures 10(a) and 10(b). The velocities agree very well, with only a 2 percent difference at $X/D_j = 26.7$. There is a larger difference in the hydrogen with an 8 percent difference at $X/D_j = 26.7$. It is interesting to note the faster hydrogen decay for the finite rate calculation. This, of course, implies faster mixing, and will be discussed in the next section.

Radial profiles for Case 1 are shown for axial stations of 6.7 and 18.7 diameters in figures 10(c) through 10(e). The velocities are again much the same as figure 10(c) indicates. Water mass fraction profiles likewise are much the same with a 3 percent difference in the peak height and a slight displacement in the radial location of the peak. Free hydrogen profiles indicate more variation as would be expected from figure 10(b). The largest difference in the calculations is seen in the static temperature (fig. 10(e)). At the 6.7 diameter location, a 16 percent difference in the peak temperature is found. This occurs because ignition delay affects the reaction at this location. The discrepancy gets smaller as the reaction proceeds; at X/D_j = 18.7 the difference is less than 10 percent.

Similar plots of Case 3 velocity, concentration, and temperature profiles are given in figure 11. Here the equilibrium and combined equilibrium and finite rate calculations are compared. Qualitatively, the same observation is made; velocities match well, but concentration and temperature results can be significantly different.

The implications of these plots relative to the acceptability of pitot pressure for mixing and reacting data/theory comparisons are twofold. First, even though figures 6 and 7 show differences in pitot pressure for similar cases with different reaction models, these differences are much less significant than differences in temperature and composition. This emphasizes the need for temperature or composition data to compare with the theory. The latter is the logical choice since concentrations are relatively easy to measure (ref. 31), but temperature would appear to be the most sensitive indicator for reacting flows. Developing optical techniques for temperature measurement therefore offers very attractive potential. Second, pitot pressure and velocity appear to have approximately the same computational sensitivity. The substitution of pitot pressure for velocity in data/theory comparisons therefore appears to be reasonable.

Mixing Rates

The ramifications of the differences in the sensitivity plots become very apparent when an attempt is made to examine mixing and combustion efficiencies. Mixing efficiency is defined as the fraction of injected hydrogen that would react if complete chemical reaction occurred without further mixing. Combustion efficiency is the fraction of injection hydrogen that actually reacts to form water. These are integral quantities at each axial station and are plotted as functions of X/D_j in figure 12. For the high temperature cases, predicted combustion efficiencies (η_c) with equilibrium and finite rate chemistry are virtually the same beyond the ignition zone. Mixing efficiencies (η_m), however, are higher for the finite rate model. Fastest mixing occurred when there was no reaction at all. Note that $\eta_c \cong \eta_m$ for the equilibrium calculations.

The low-temperature results show amplified effects of finite rate chemistry (figure 12(b)). Here again combustion efficiencies are much the same for the equilibrium and finite rate models after the ignition zone. Mixing efficiencies are again higher for the finite rate model. Highest

mixing and combustion efficiencies were achieved with the combined chemistry model utilizing finite rate ($0 < X/D_j < 6.7$) and equilibrium ($X/D_j > 6.7$).

It is obvious that the prediction of the development of the flow in the first several diameters is critical. Downstream mixing rates ($d\eta_m/d\ X/D$) are very nearly the same for the low temperature equilibrium and combined calculations, but are quite different in the first few diameters. A similar observation can be made for the high temperature calculations. The implication of these results is clear; reaction appears to have an adverse effect on mixing in the region close to the point of injection. This is in apparent disagreement with physical arguments that reaction should enhance the turbulence, and therefore enhance mixing. Unfortunately, resolution of this matter is not possible without sufficient concentration measurements to determine the exact location of the hydrogen for each case.

One additional point regarding calculated mixing rates is appropriate. Combustion efficiencies predicted for the ducted flows (Cases 4 and 5) are identical to those predicted for Cases 1 and 2. The degree of the adverse pressure gradient present in the ducted flows was therefore found to have no appreciable effect on the computed rate of mixing.

CONCLUDING REMARKS

Pitot pressure results from a coaxial hydrogen/air mixing and reacting experiment have been correlated using a parabolic mixing program with constant turbulent Prandtl and Lewis numbers and an eddy viscosity model developed from cold-flow mixing. Good agreement was found for both reacting and non-reacting cases with the same value of the empirical constant; the viscosity model, therefore appears capable of handling the large density differences induced by combustion. Use of a finite rate chemistry model enabled the computation of ignition delay, but after ignition equilibrium chemistry gave the best representation of the data.

Ducted pitot and static pressure results were correlated with the same theory and viscosity formulation as were used for free-jet calculations. Agreement was generally good, but the potential of the analysis appears to be limited by the coordinate system (stream function) and the handling of the boundary conditions.

Comparison of computed velocity, concentration, and temperature results for the various cases showed pitot pressure to be a valid quantity for data/theory comparison. The sensitivity of pitot pressure was comparable to that of velocity. The need for other comparisons was apparent, however, as concentration and temperature were found to differ significantly, even when pitot pressure and velocity did not.

Mixing and combustion efficiency calculations implied an adverse effect of reaction on mixing in the first few injector diameters. Based on the sensitivity results, however, confirmation of this result awaits more extensive data.

REFERENCES

1. Henry, J. R.; and Anderson, G. Y.: Design Considerations for the Airframe-Integrated Scramjet. Presented at First International Symposium on Air-Breathing Engines (Marseille, France), June 1972.

2. Henry, J. R.; and Beach, H. L.: Hypersonic Air-Breathing Propulsion Systems. Paper No. 8, NASA SP-292, November 1971.

3. Ferri, A.: Review of Scramjet Propulsion Technology. J. Aircraft, Vol. 5, No. 1, Jan.-Feb. 1968, p. 3.

4. Anderson, G. Y.: An Examination of Injector/Combustor Design Effects on Scramjet Performance. Presented at Second International Symposium on Air-Breathing Engines (Sheffield, England), March 1974.

5. Becker, J. V.: New Approaches to Hypersonic Aircraft. Presented at the Seventh Congress of International Council of the Aeronautical Sciences (Rome, Italy), September 1970.

6. Beach, H. L.: Supersonic Mixing and Combustion of a Hydrogen Jet in a Coaxial High-Temperature Test Gas. AIAA Paper 72-1179, December 1972.

7. Harsha, P. T.: Free Turbulent Mixing: A Critical Evaluation of Theory and Experiment. AEDC TR 71-36, February 1971.

8. Free Turbulent Shear Flows. NASA SP-321, 1973.

9. Turbulent Mixing in Non-Reactive and Reactive Flows: Proceedings of a Workshop held at Purdue University, May 20-21, 1974; December 1974.

10. Swithenbank, J.: The Unknown Fluid Mechanics of Combustion. Fluid Mechanics of Combustion, J. L. Dussourd, R. P. Lohmann, and E. M. Uram, eds., American Society of Mechanical Engineers, 1974, pp. 1-5.

11. Poll, I.; Payne, R.; Swithenbank, J.; and Vincent, M. W.: Combustor Modelling. Presented at Second International Symposium on Air-Breathing Engines (Sheffield, England), March 1974.

12. Evans, J. S.; and Anderson, G. Y.: Supersonic Mixing and Combustion in Parallel Injection Flow Fields. Presented at AGARD Propulsion and Energetics Panel Meeting (Liege, Belgium), April 1974.

13. Eggers, J. M.; and Torrence, M.G.: An Experimental Investigation of the Mixing of Compressible Air Jets in a Coaxial Configuration. NASA TN D-5315, July 1969.

14. Eggers, J. M.: Turbulent Mixing of Coaxial Compressible Hydrogen-Air Jets. NASA TN D-6487, September 1971.

15. Anderson, G. Y.; Agnone, A. M.; and Russin, W. R.: Composition Distribution and Equivalent Body Shape for a Reacting, Coaxial, Supersonic Hydrogen-Air Flow. NASA TN D-6123, January 1971.

16. Rogers, R. C.: A Study of the Mixing of Hydrogen Injected Normal to a Supersonic Airstream. NASA TN D-6114, March 1971.

17. Rogers, R. C.: Mixing of Hydrogen Injected from Multiple Injectors Normal to a Supersonic Airstream. NASA TN D-6476, September 1971.

18. McClinton, C. R.: The Effect of Injection Angle on the Interaction between Sonic Secondary Jets and a Supersonic Free Stream. NASA TN D-6669, February 1972.

19. Cohen, L. S.; and Guile, R. N.: Investigation of the Mixing and Combustion of Turbulent, Compressible Free Jets. NASA CR-1473, Dec. 1969.

20. Drewry, J. M.: Supersonic Mixing and Combustion of Coaxial Hydrogen-Air Streams in a Duct. ARL 71-0286, December 1971.

21. Cookson, R. A.; Flanagan, P.; and Perry, G. S.: A Study of Free-Jet and Enclosed Supersonic Diffusion Flames. Twelfth Symposium (International) on Combustion, pp. 1115-1124, The Combustion Institute, 1969.

22. Trout, O. F.: Design, Operation, and Testing Capabilities of the Langley 11-Inch Ceramic-Heated Tunnel. NASA TN D-1598, February 1963.

23. Sutton, K.: Descriptions and Operating Parameters of a Mach 2 Nozzle System for the Langley 11-Inch Ceramic-Heated Tunnel. NASA TN D-4750, September 1968.

24. Clippinger, R. F.: Supersonic Axially Symmetric Nozzles, Rept. No. 794, Ballistic Research Laboratory, Aberdeen Proving Ground, December 1951.

25. Casaccio, A.; and Rupp, R. L.: A Supersonic Combustion Test Program Utilizing Gas Sampling, Optical, and Photographic Measuring Techniques. NASA CR-66393, July 1967.

26. Ededman, R.: Diffusion Controlled Combustion for Scramjet Application. Part I - Analysis and Results of Calculations. Tech. Rep. 569 (Contract No. NASL-5117), Gen. Appl. Sci. Lab., Inc., December 1965.

27. Hopf, H.; and Fortune, O.: Diffusion Controlled Combustion for Scramjet Application. Part II - Programmer's Manual. Tech. Rep. 569 (Contract No. NAS1-5117), Gen. Appl. Sci. Lab., Inc., December 1965.

28. Moretti, G.: A New Technique for the Numerical Analysis of Nonequilibrium Flows. AIAA J., Vol. 3, No. 2, February 1965, pp. 223-229.

29. Abett, M. J.: Users Manual for the One-Dimensional Fluid Flow, Finite Rate Chemical Kinetics Program with Specified Pressure or Area for the Hydrogen-Air System. Tech. Rep. 597, Gen. Appl. Sci. Lab., Inc., February 1966.

30. Patankar, S. V.; and Spalding, D. B.: Heat and Mass Transfer in Boundary Layers. Second Ed. Intertext Books (London), 1970.

31. Beach, H. L.: Evaluation of a Wedge Gas-Sampling Probe. AIAA J., Vol. 12, No. 9, September 1974, pp. 1284-1286.

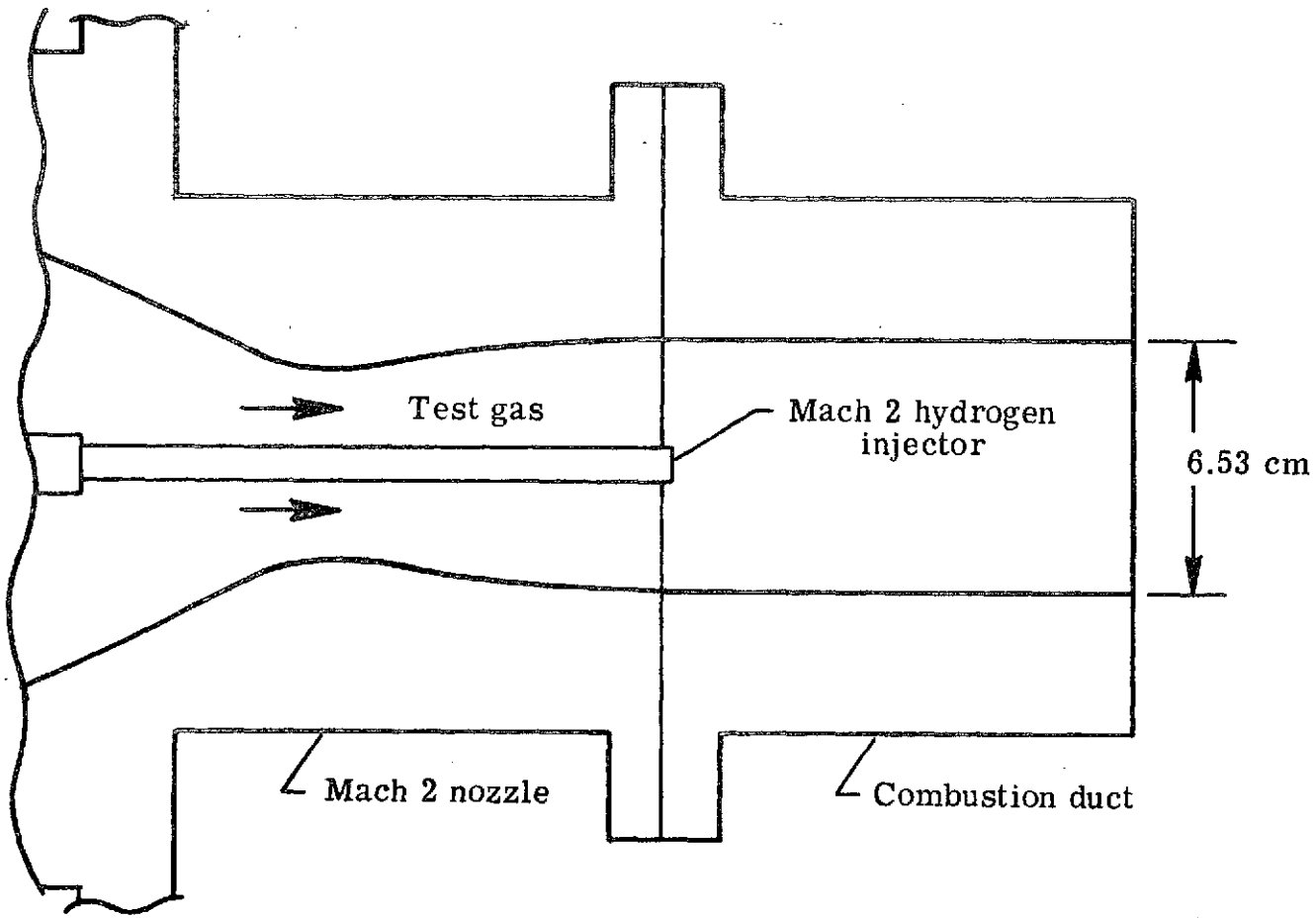

Figure 1.- Schematic of experimental apparatus.

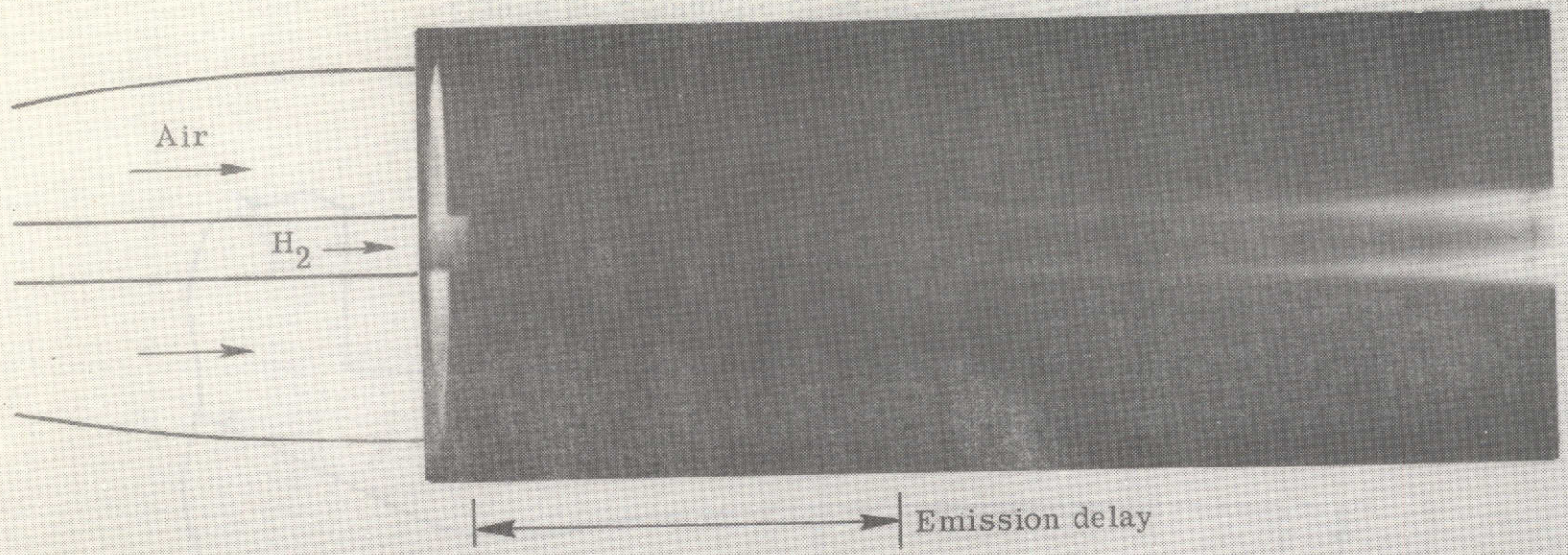

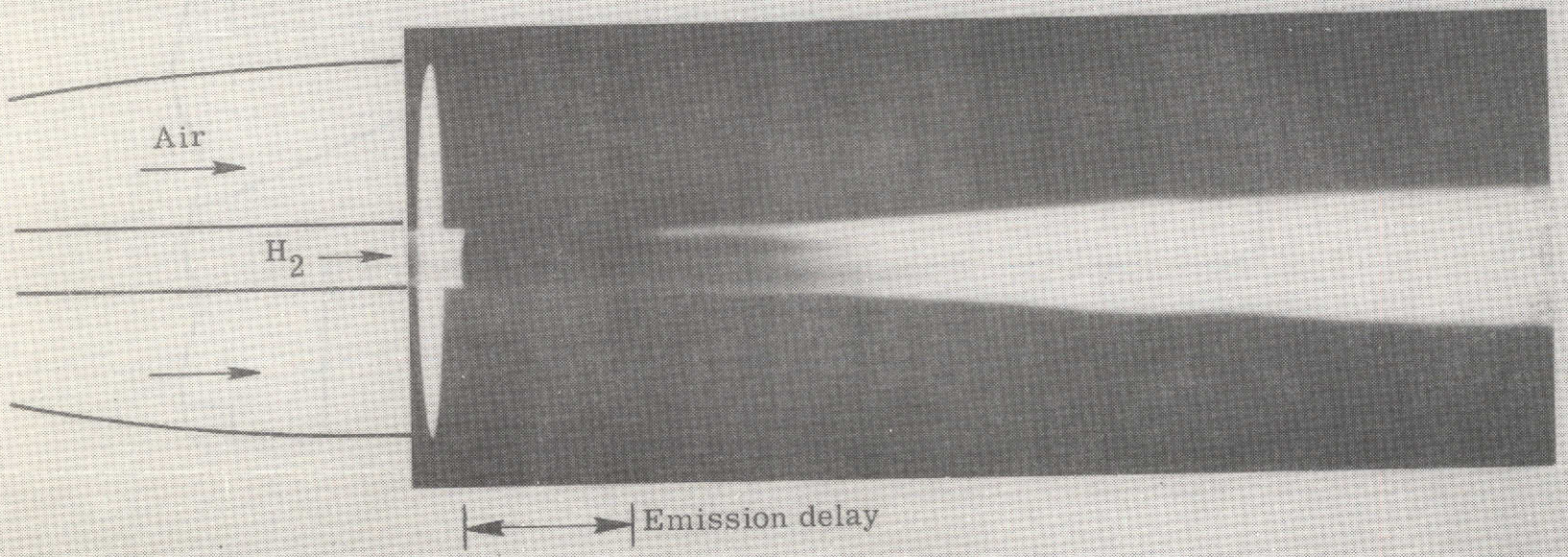

Figure 2.- Reacting flowfields.

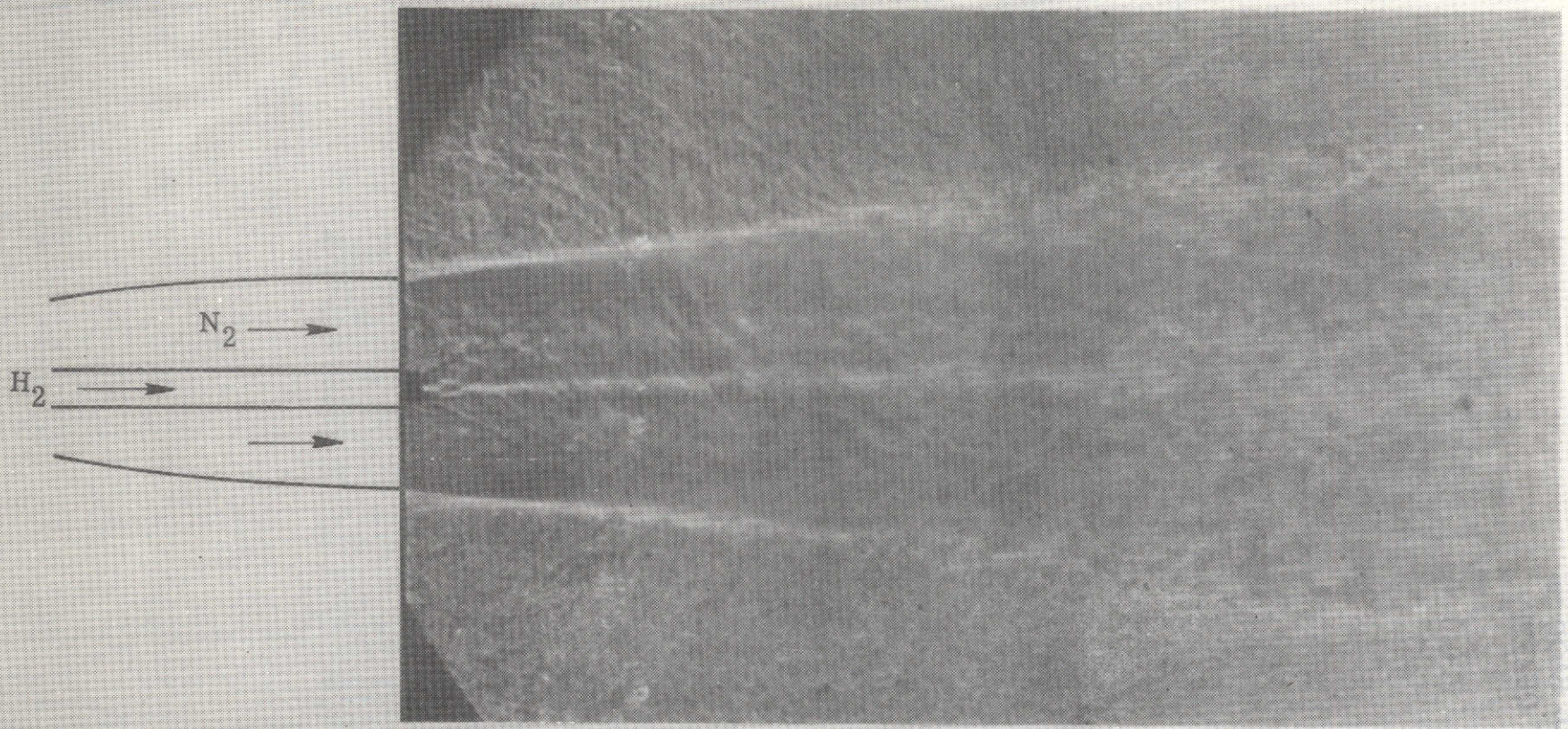

(b) Case 2; high temperature non-reacting.

Figure 3.- Continued.

(c) Case 3; low temperature reacting.

Figure 3.- Concluded.

(a) Case 1; high temperature reacting.

Figure 3.- Flowfield shadowgraphs.

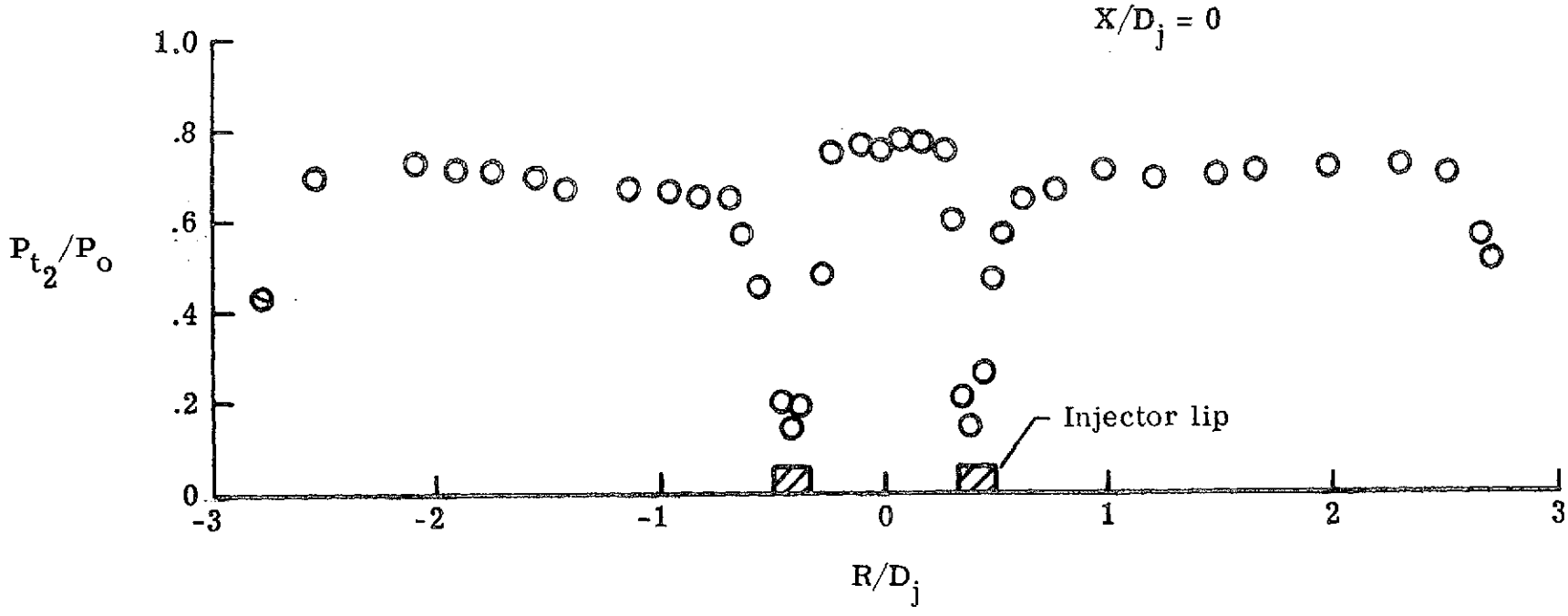

Figure 4.- Exit pitot pressure survey.

Total temperature assumption	Calculated ignition delay (X/D_j)	
	Case 1	Case 3
1	1.0	5.6
2	2.5	6.3
3	9.5	-
4	-	-

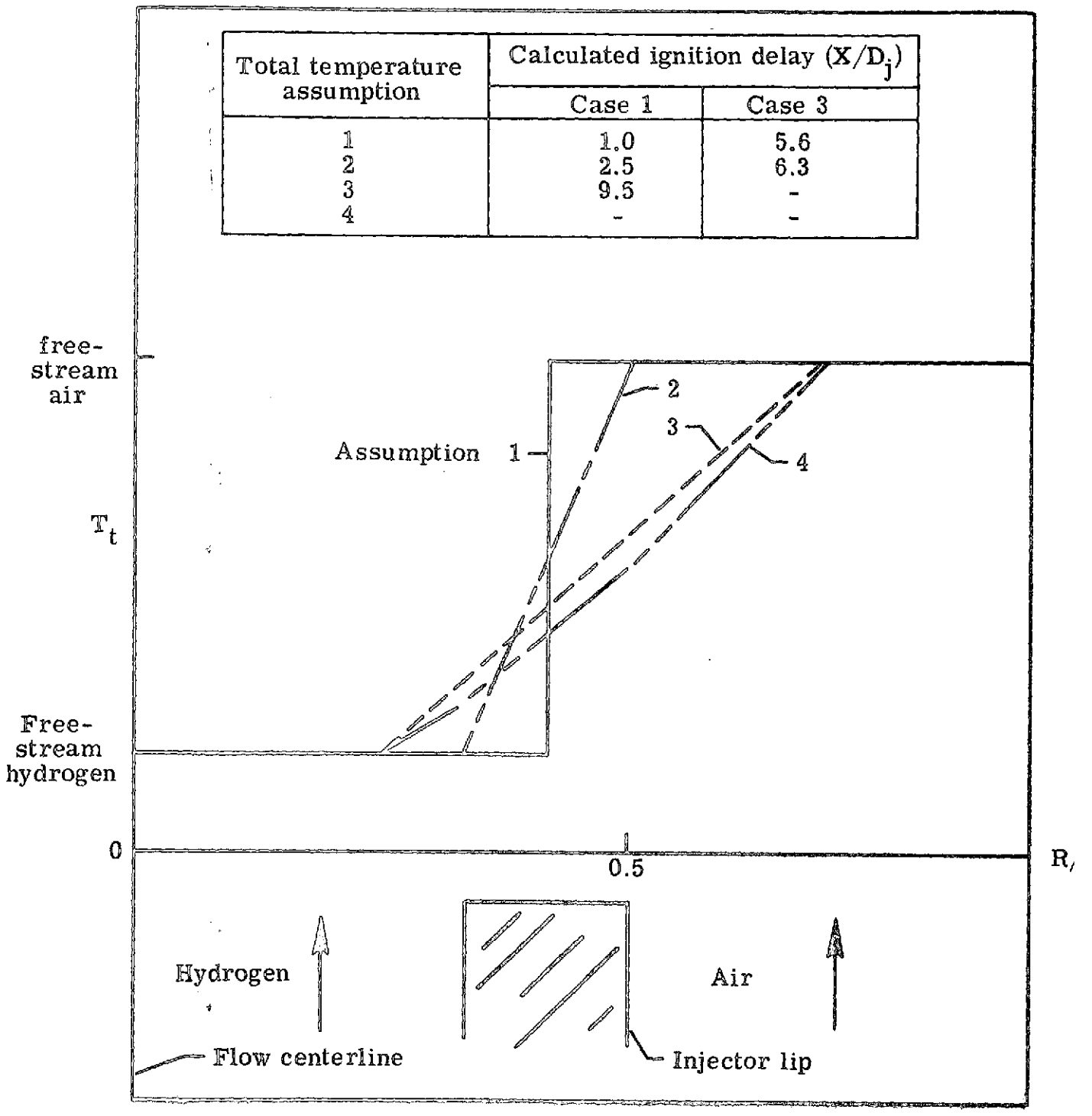

Figure 5.- Total temperature assumption.

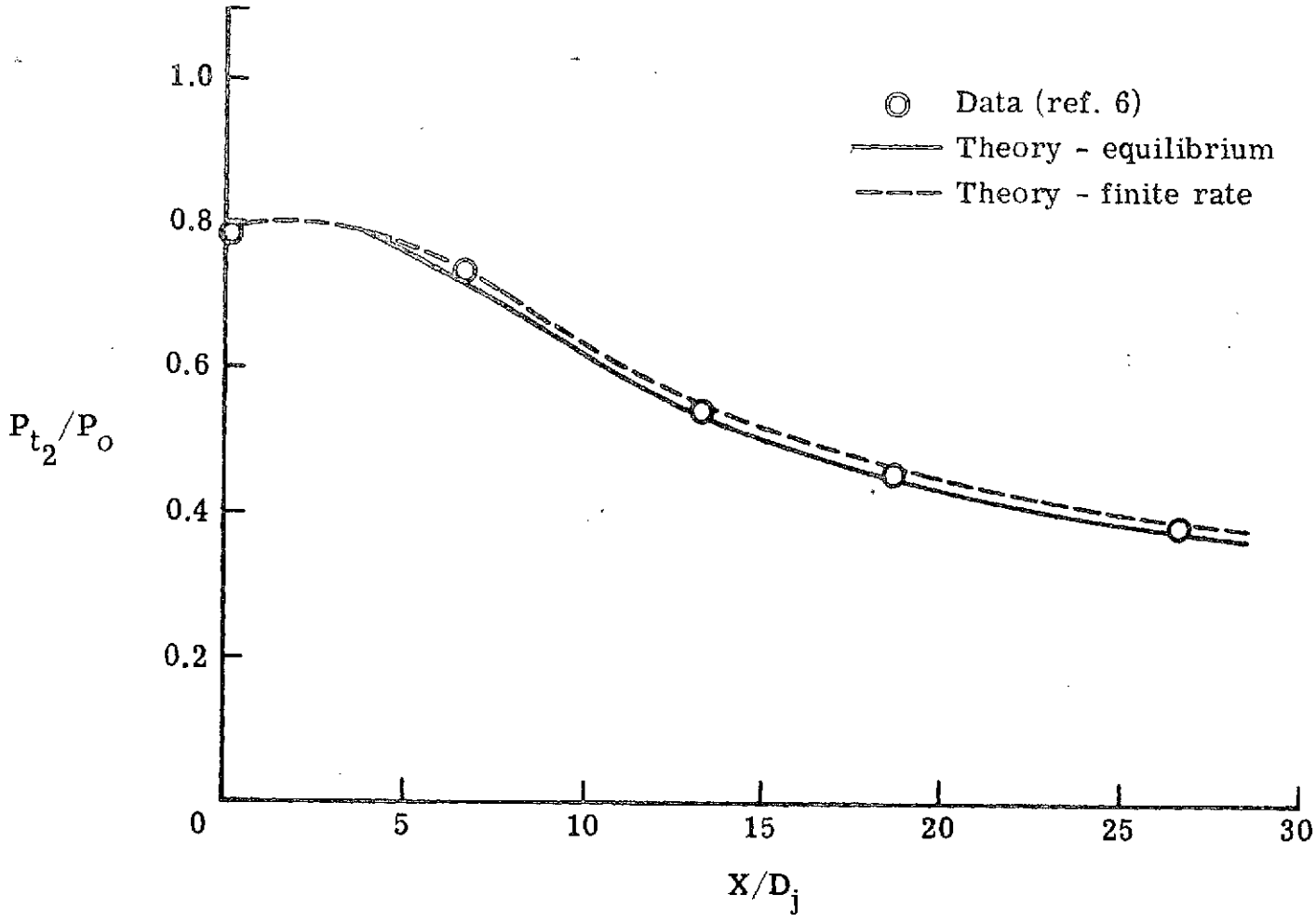

(a) Case 1; high temperature reacting.

Figure 6.- Centerline variation of free-jet pitot pressure.

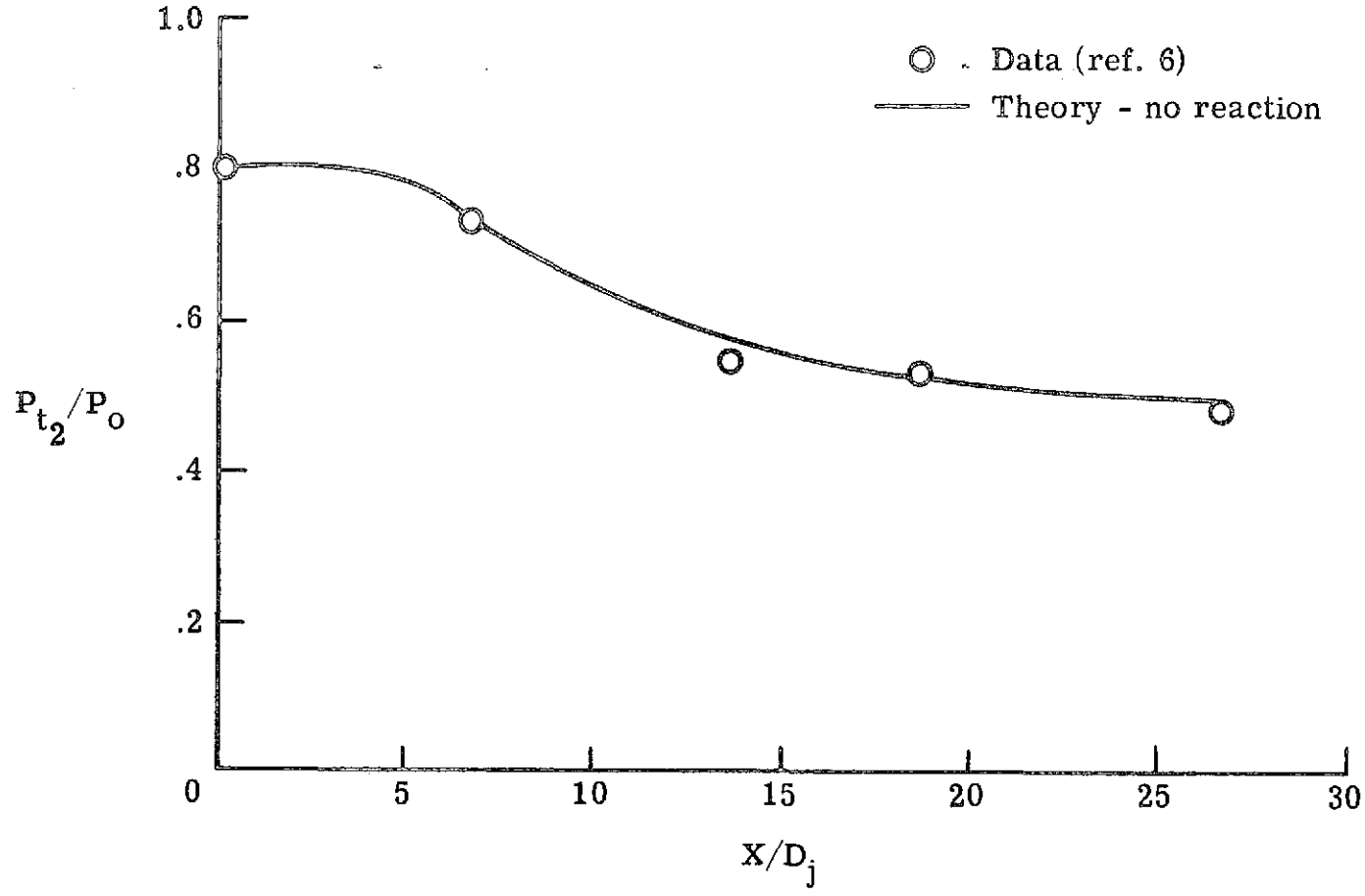

(b) Case 2; high temperature non-reacting.

Figure 6.- Continued.

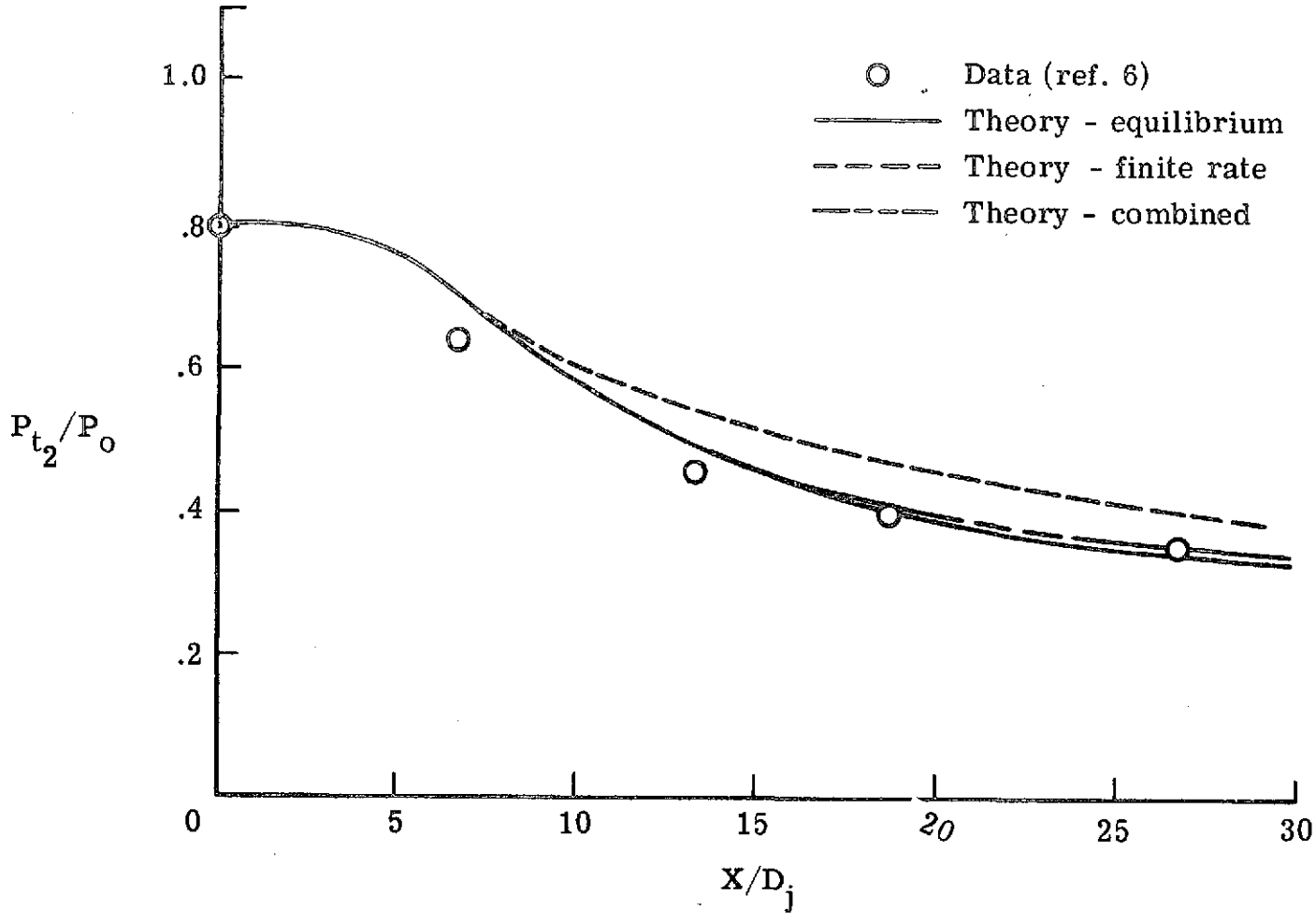

(c) Case 3; low temperature reacting.

Figure 6.- Concluded.

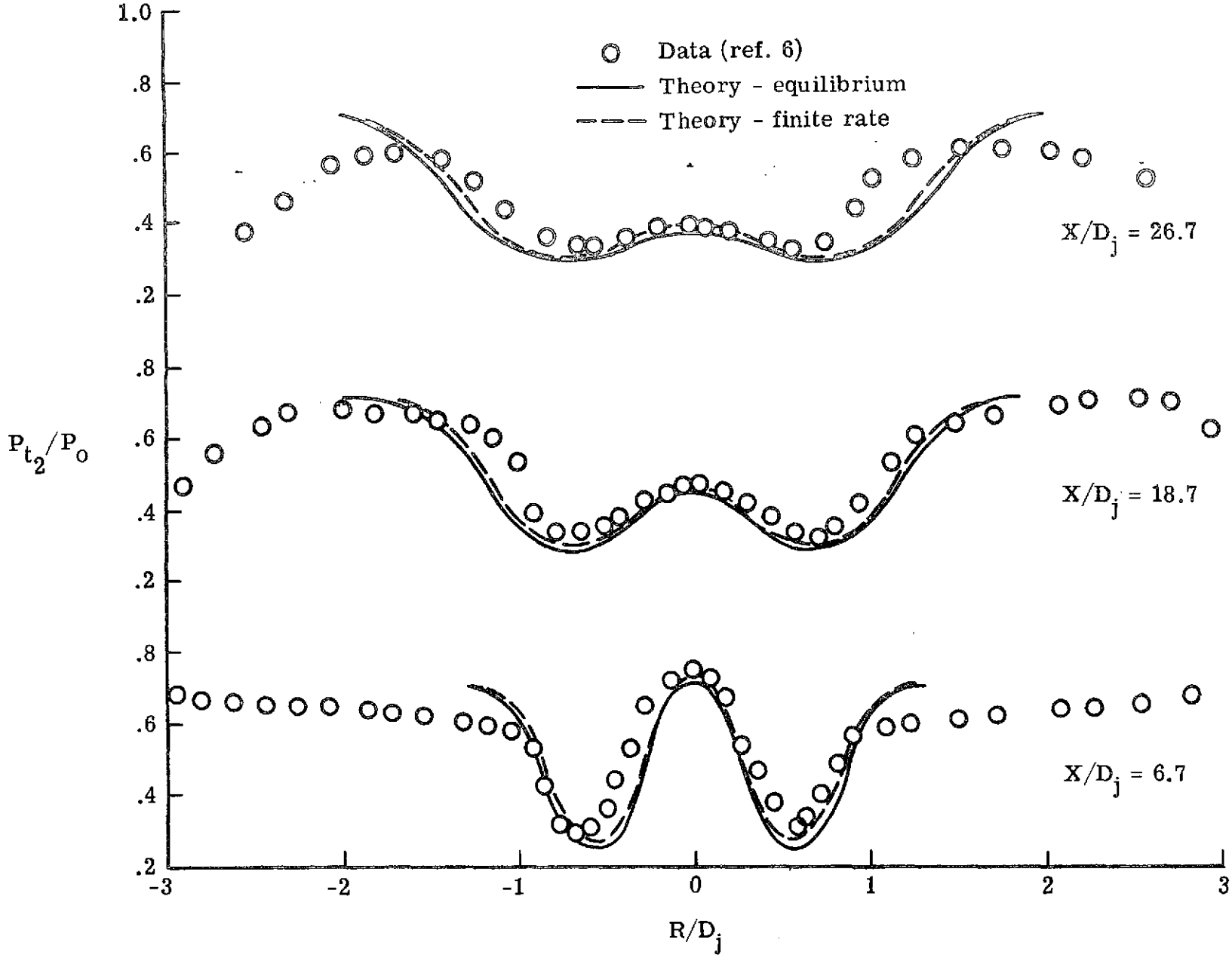

(a) Case 1; high temperature reacting.

Figure 7.- Radial variation of free-jet pitot pressure.

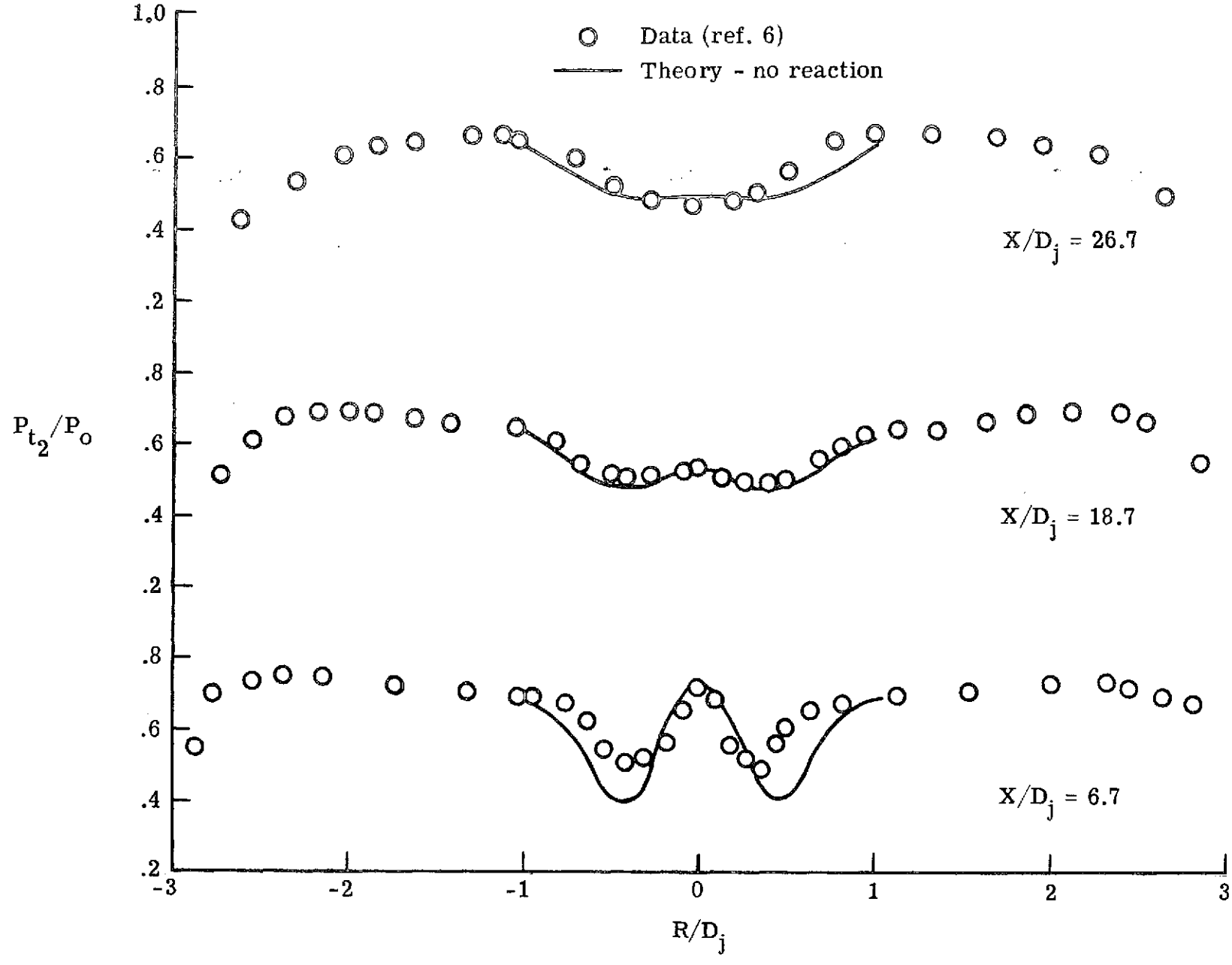

(b) Case 2; high temperature non-reacting.

Figure 7.- Continued.

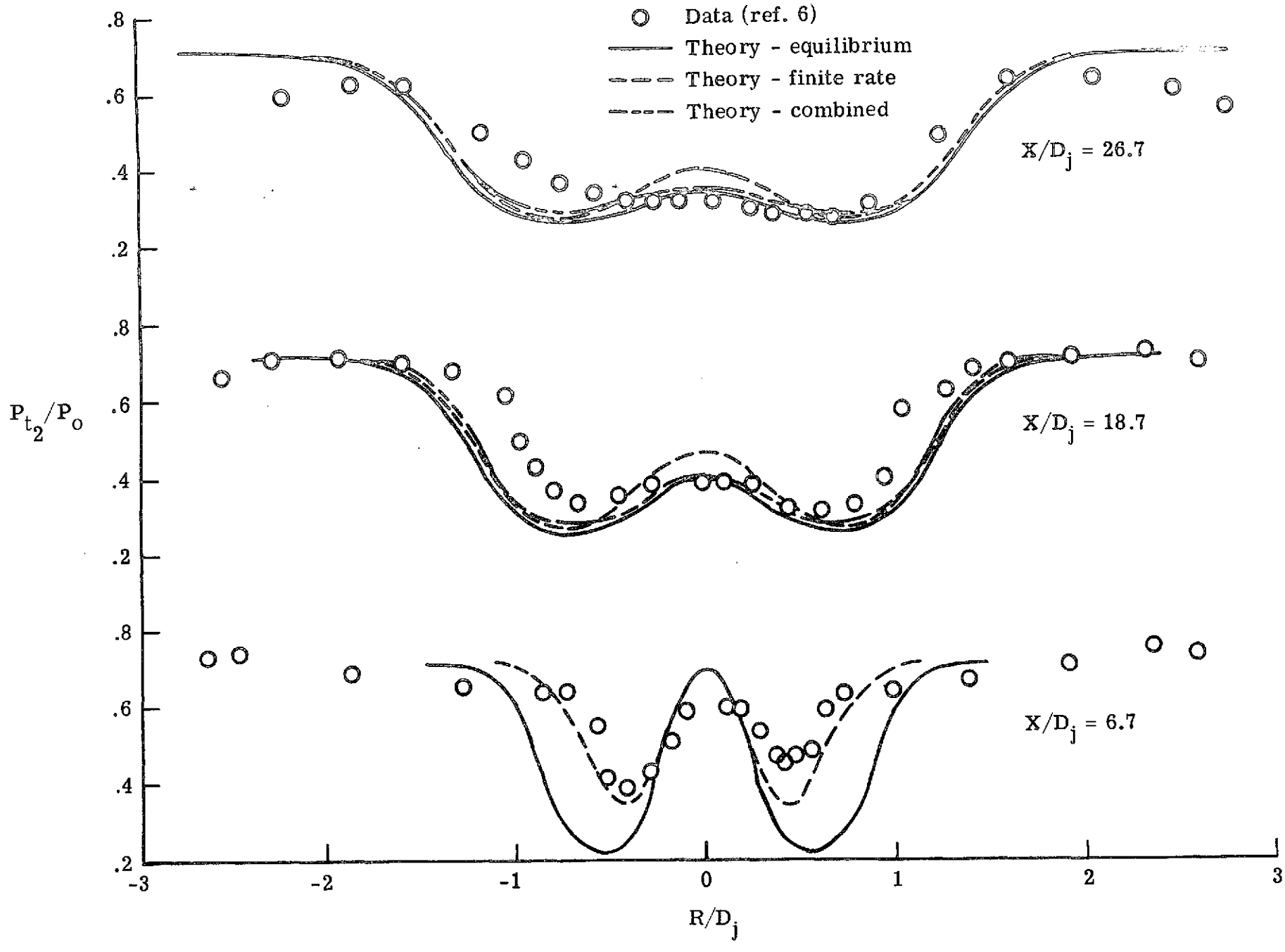

(c) Case 3; low temperature reacting.

Figure 7.- Concluded.

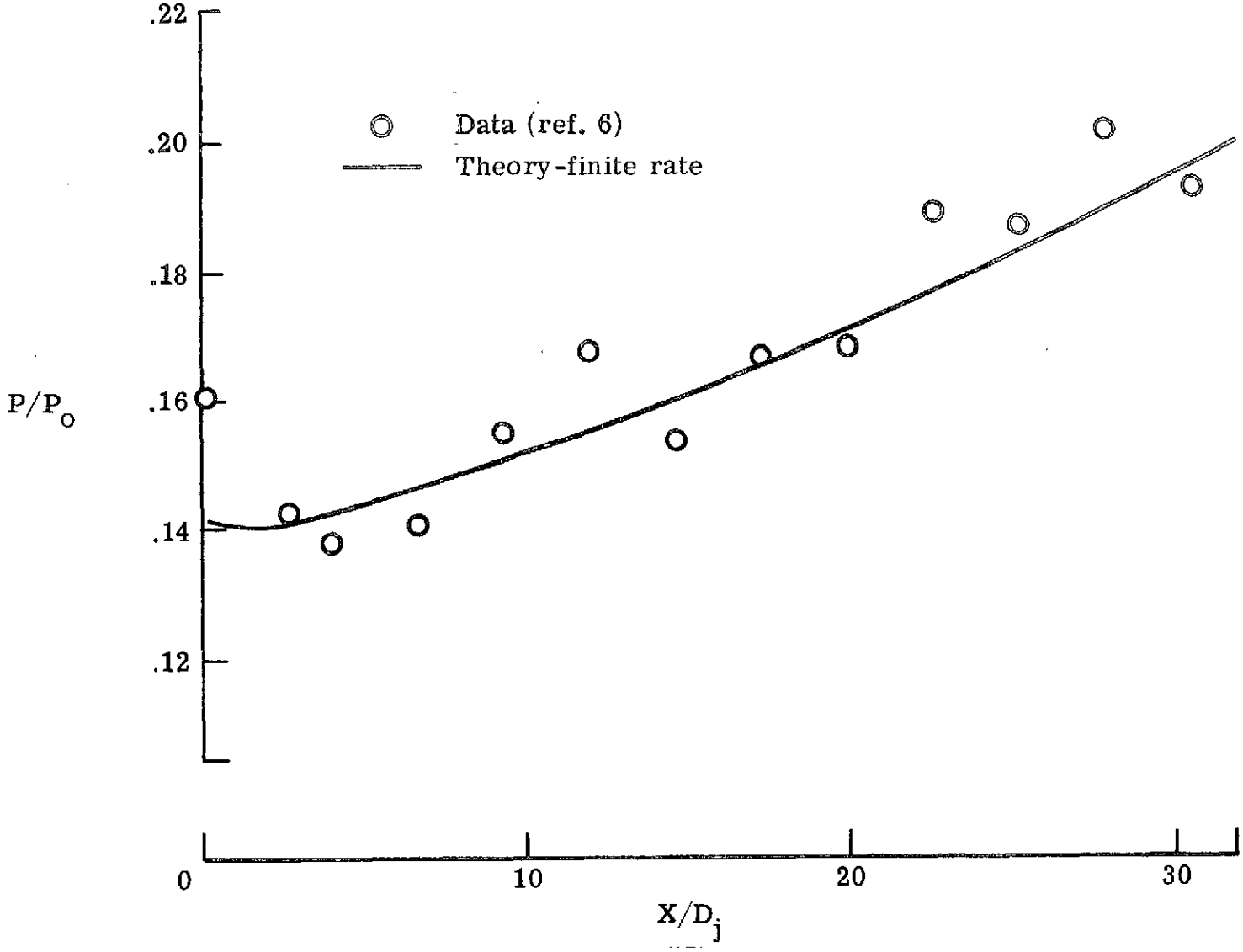

(a) Case 4; 30.5 cm duct.

Figure 8.- Wall static pressure distributions.

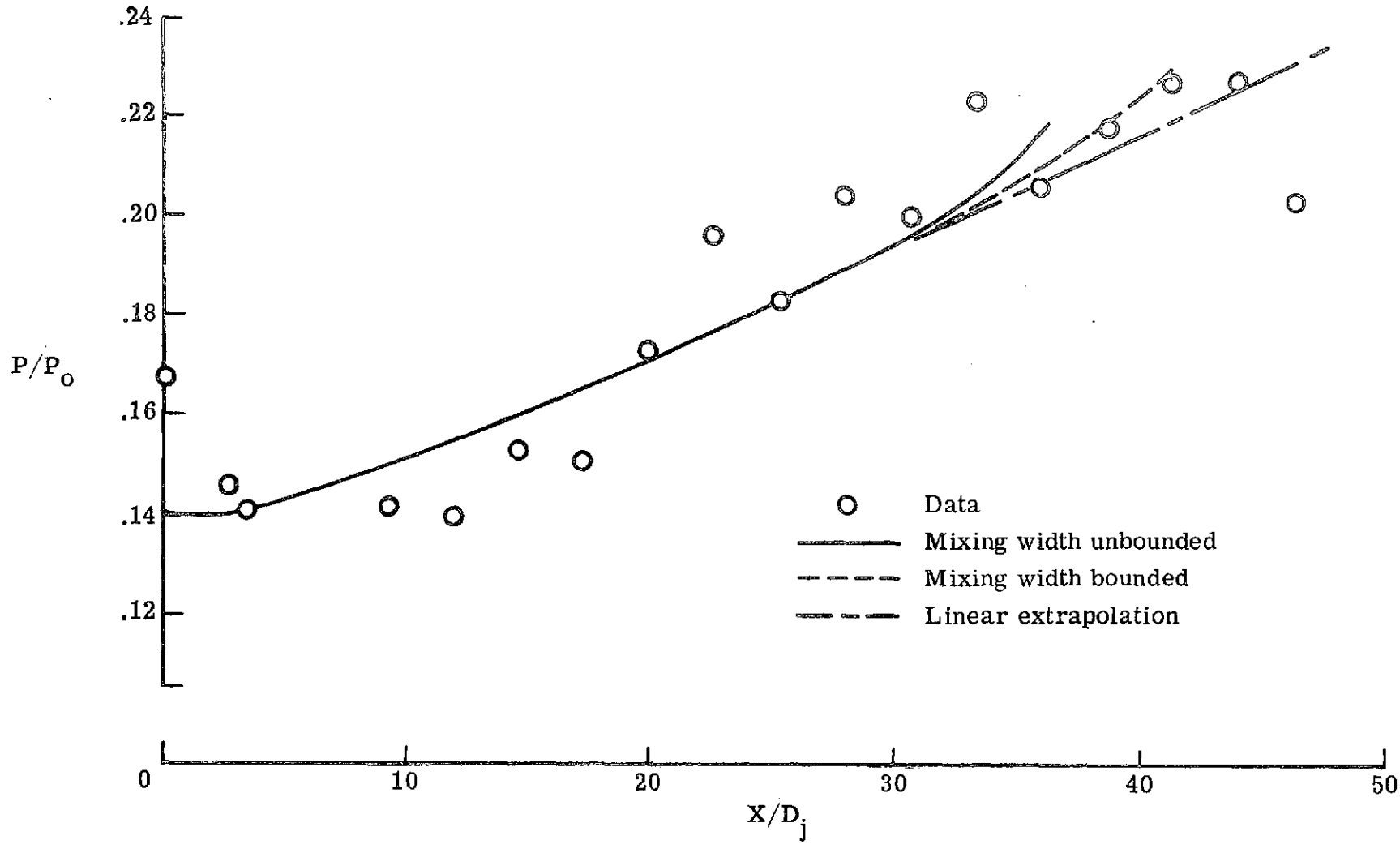

(b) Case 4; 45.7 cm duct.

Figure 8.- Continued.

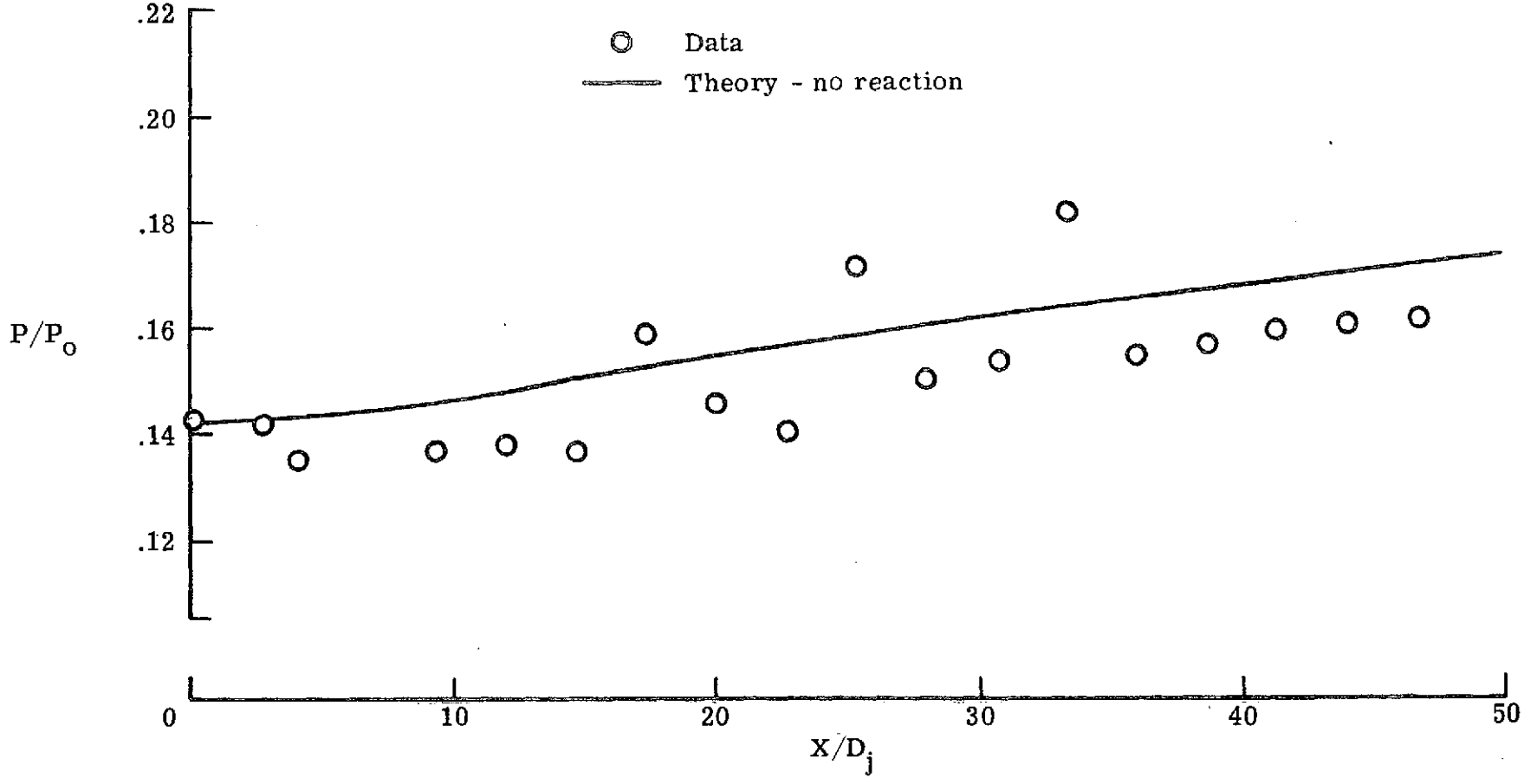

(c) Case 5; 45.7 cm duct.

Figure 8.- Concluded.

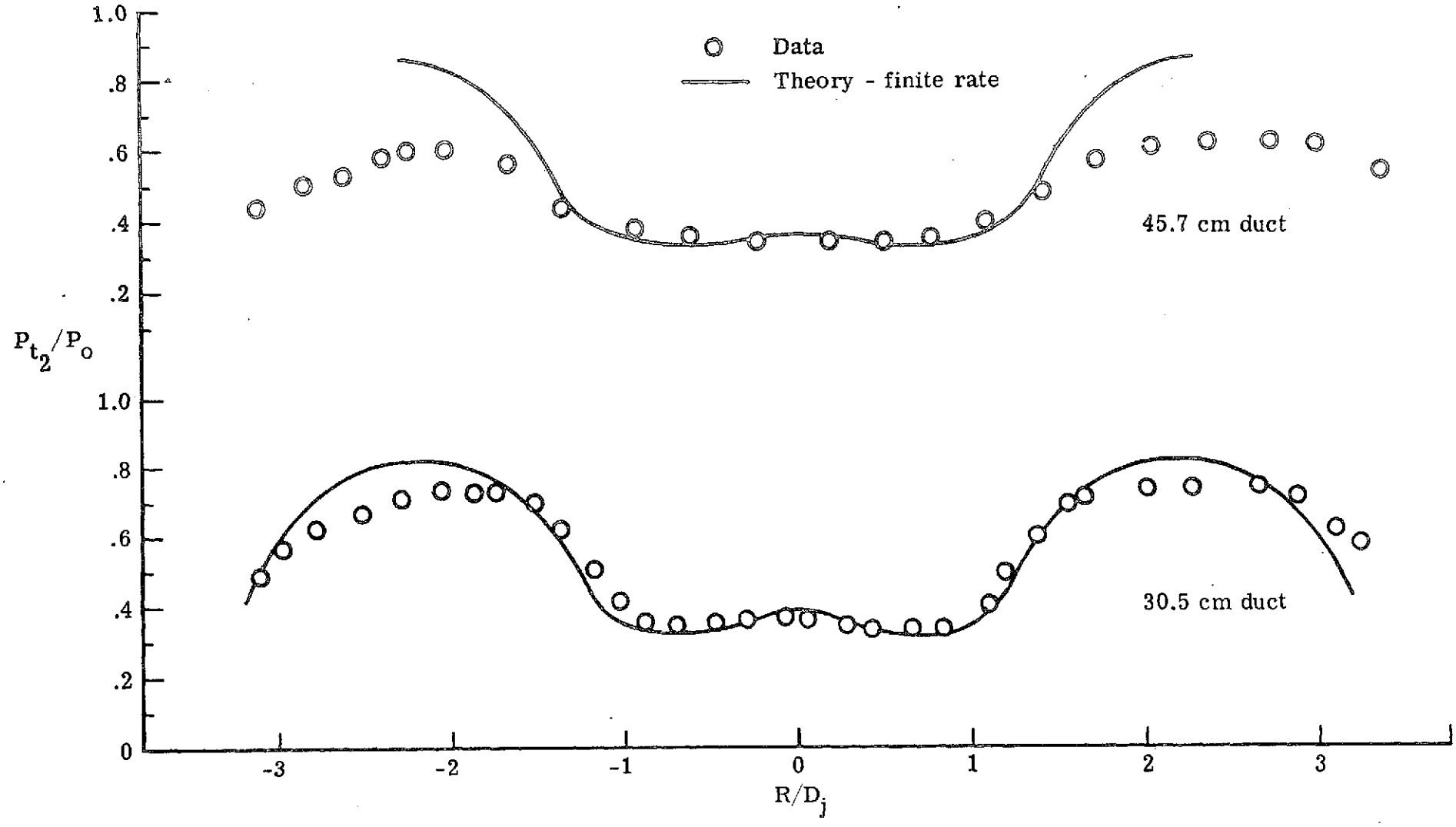

(a) Case 4; high temperature reacting.

Figure 9.- Radial variation of ducted pitot pressure.

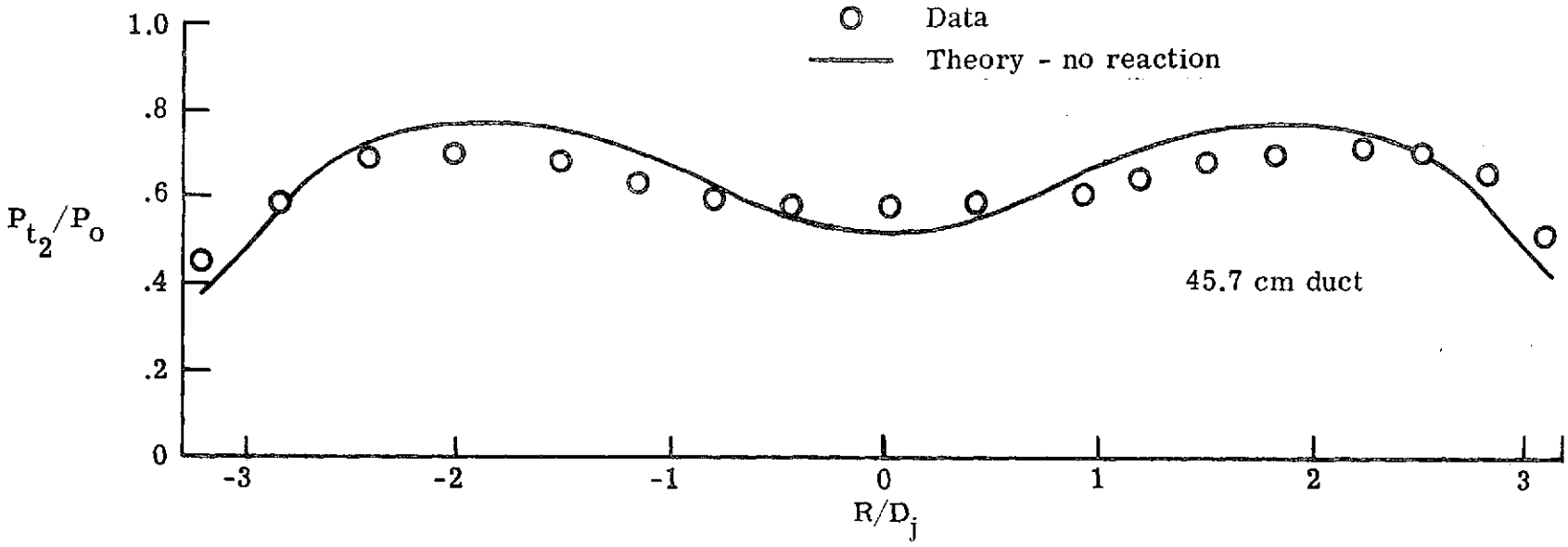

(b) Case 5; high temperature non-reacting.

Figure 9.- Concluded.

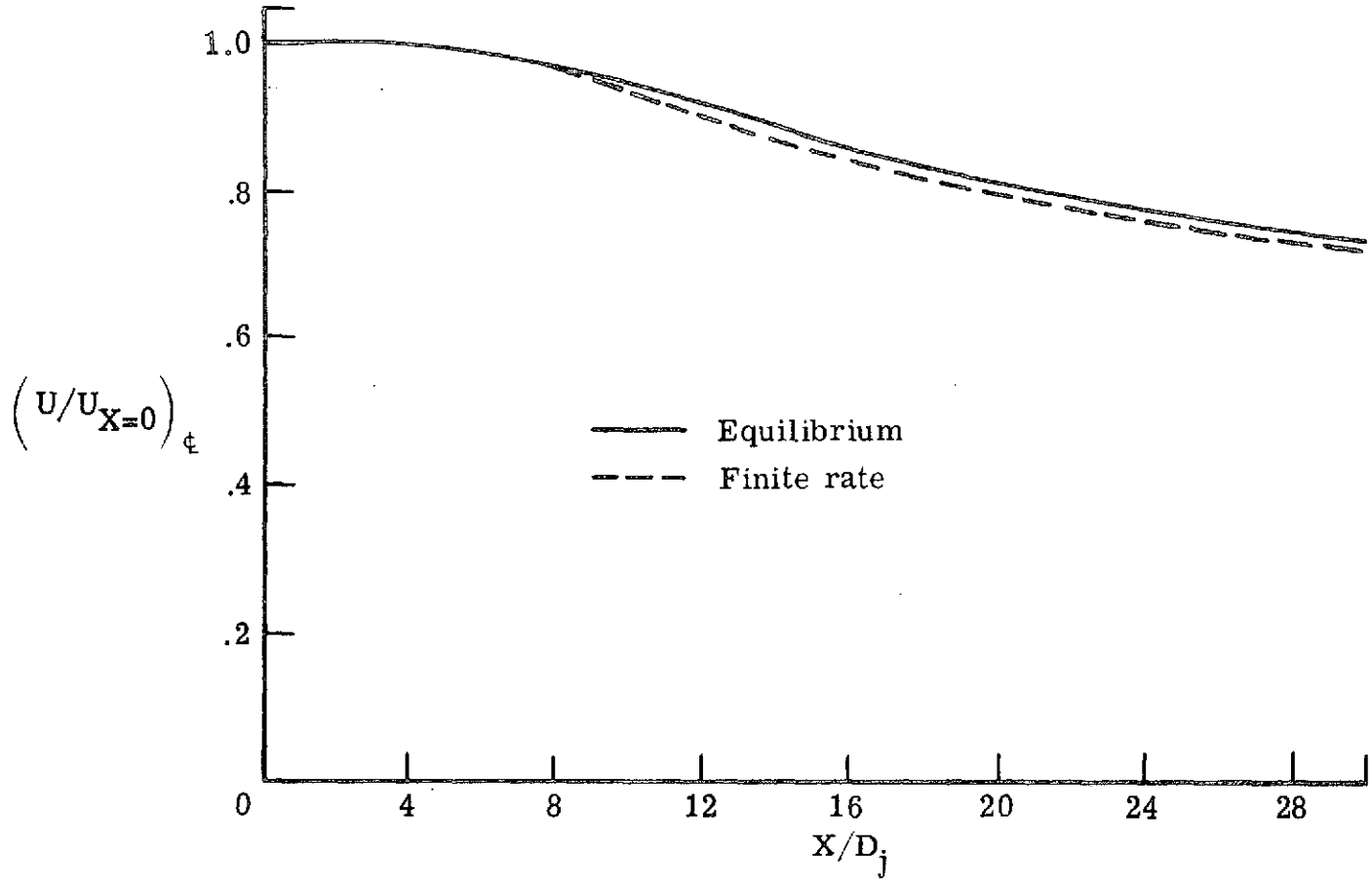

(a) Centerline velocity decay.

Figure 10.- Comparison of high temperature reacting calculations with equilibrium and finite rate chemistry.

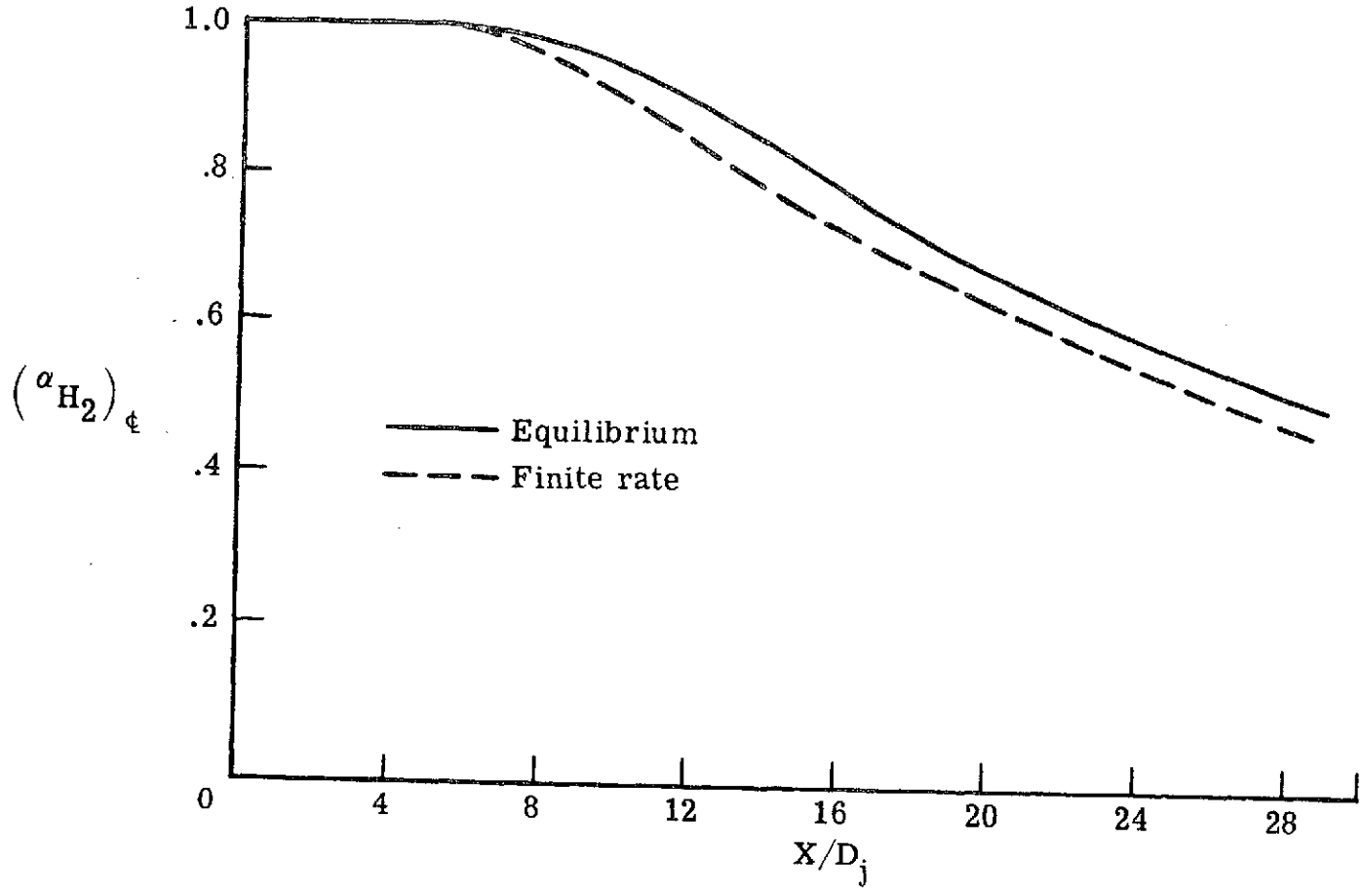

(b) Centerline decay of unreacted hydrogen.

Figure 10.- Continued.

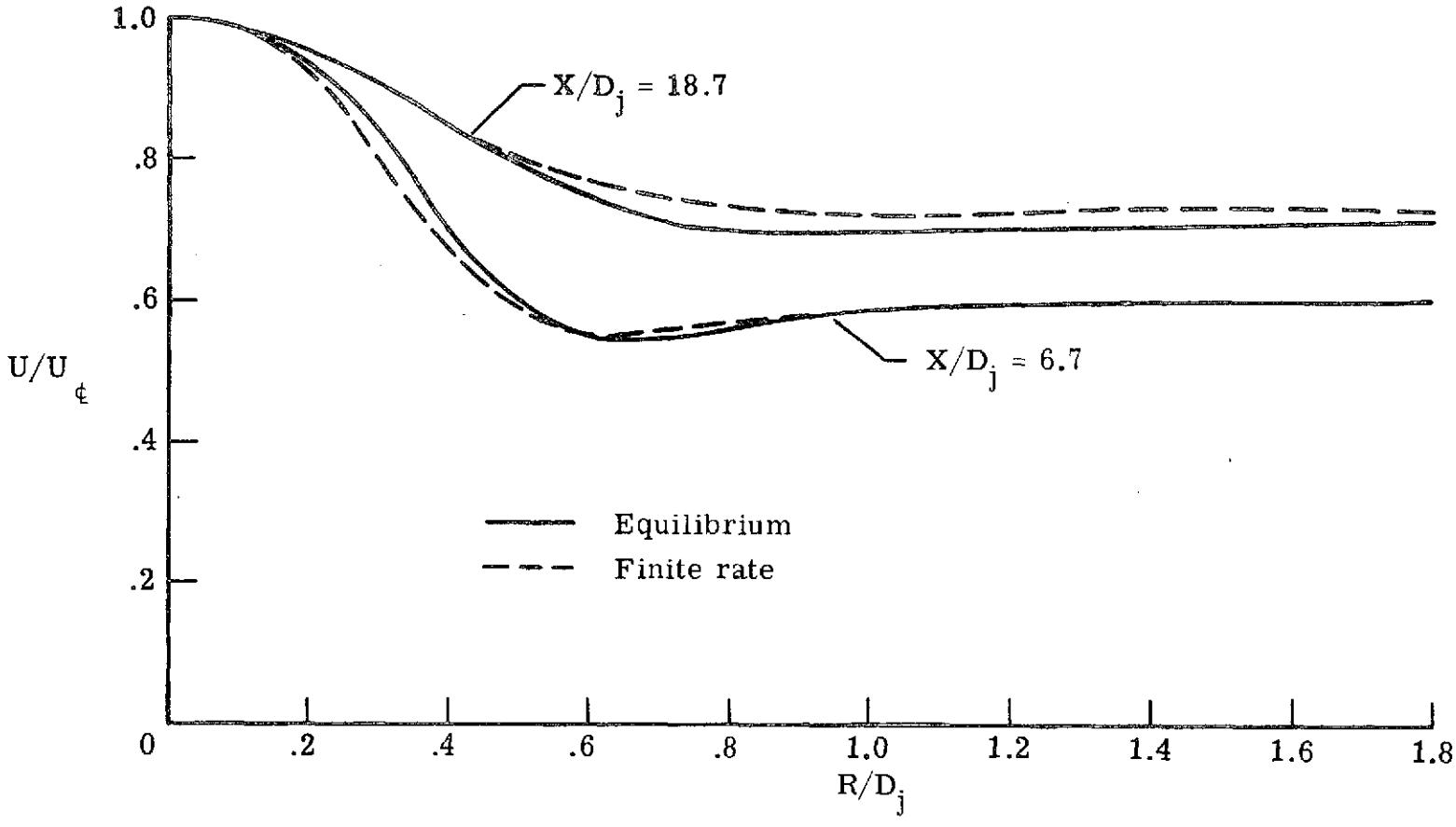

(c) Radial variation of velocity.

Figure 10.- Continued.

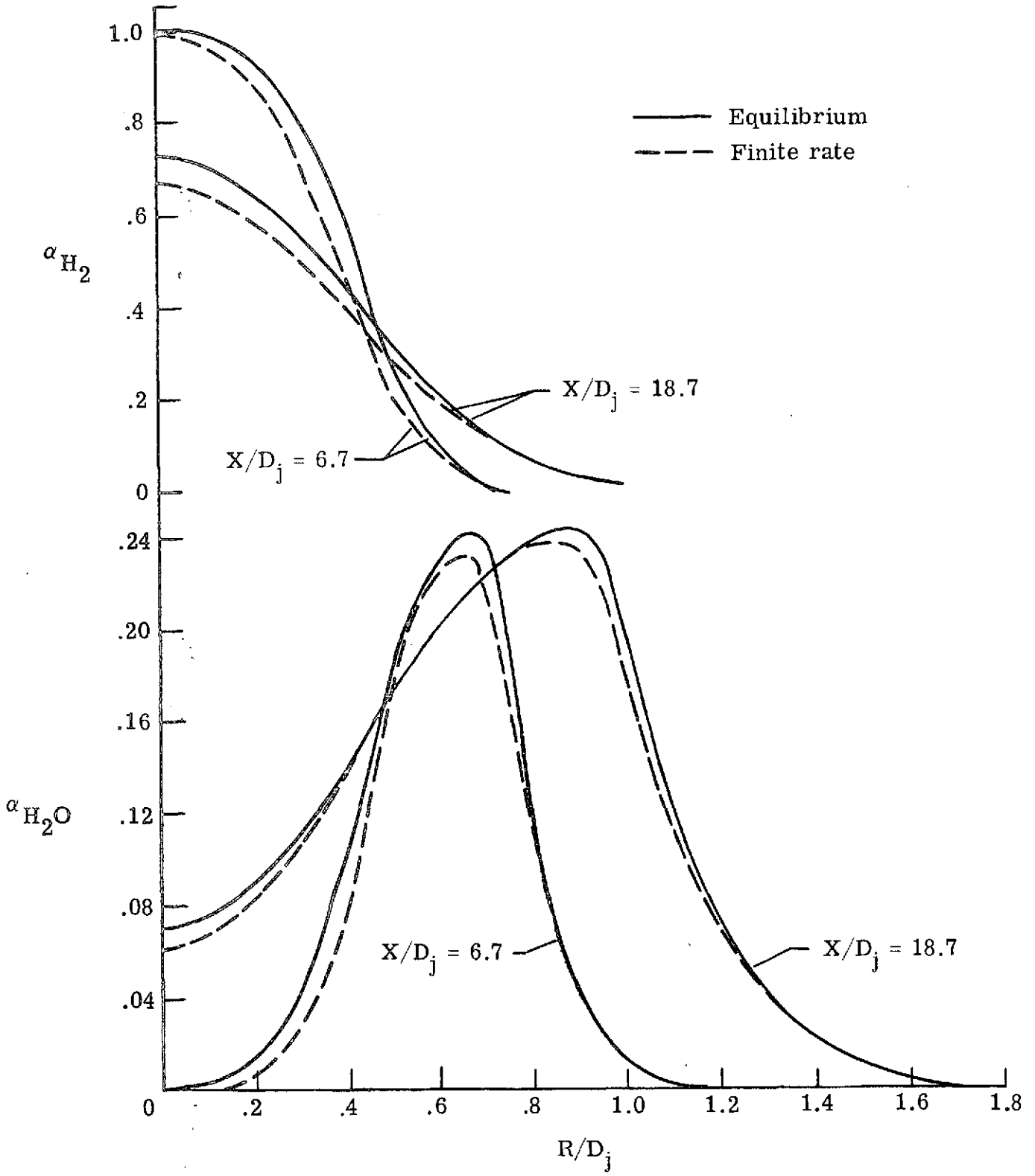

(d) Radial variation of concentration.

Figure 10.- Continued.

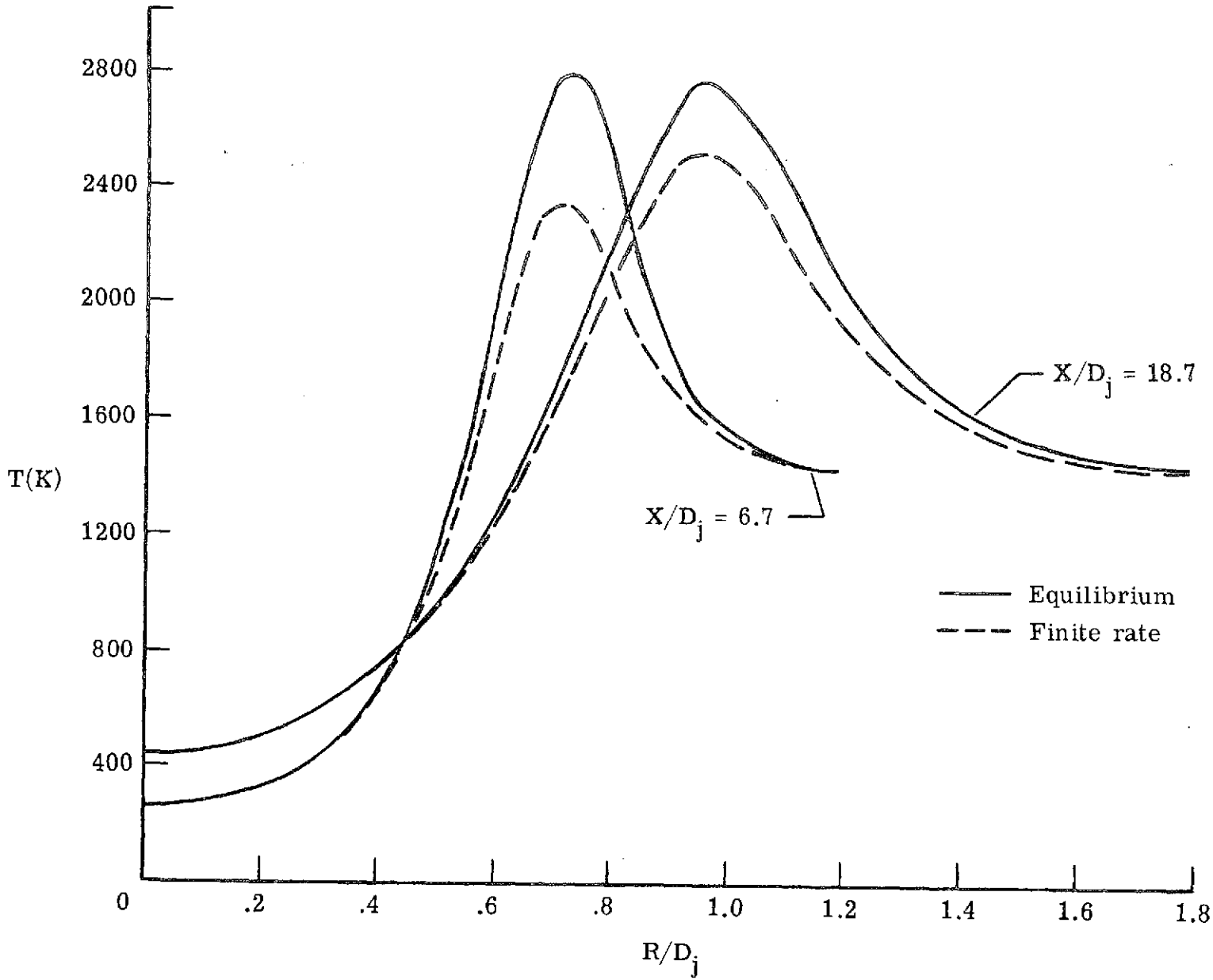

(e) Radial variation of static temperature.

Figure 10.- Concluded.

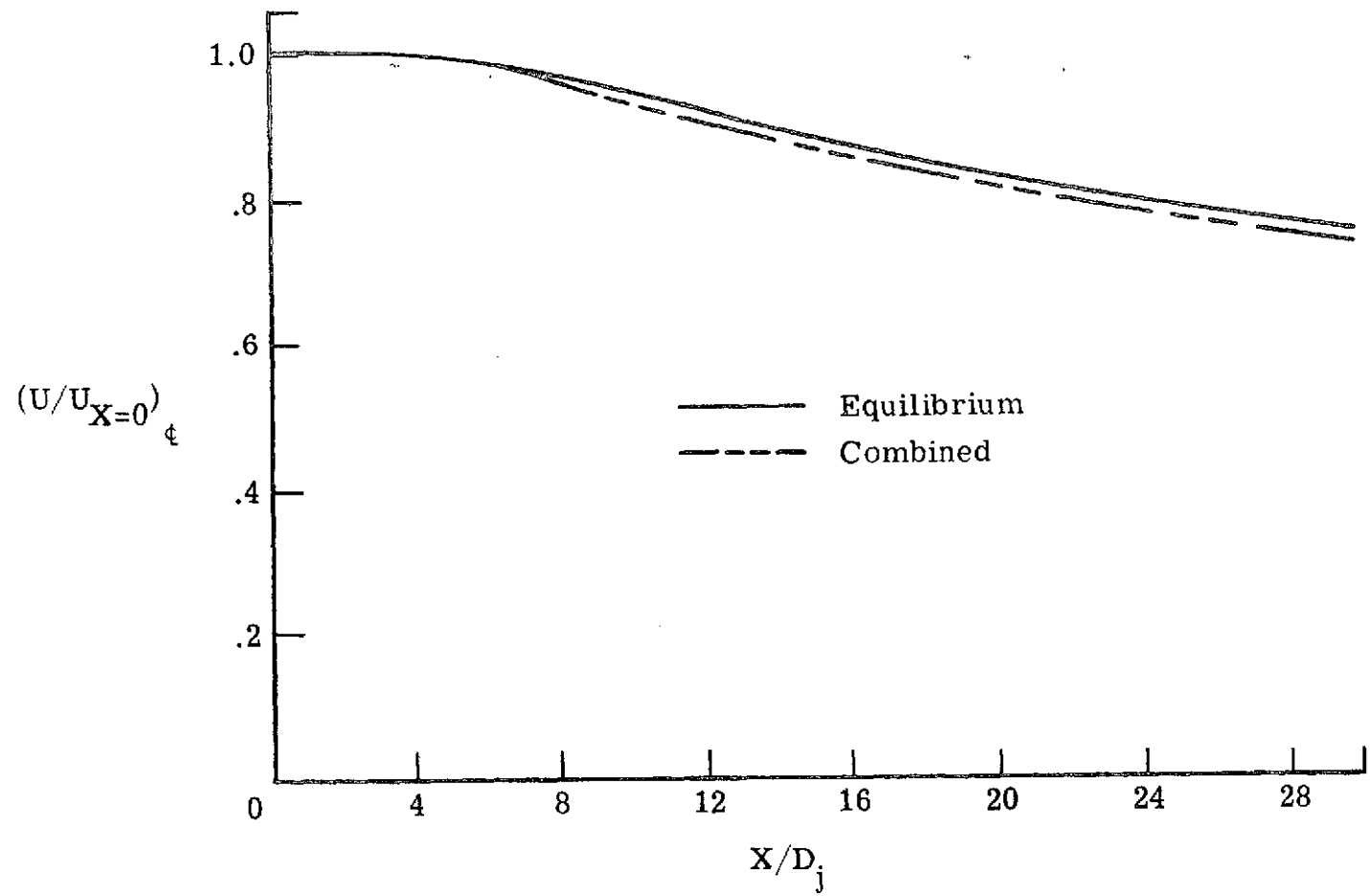

(a) Centerline velocity decay.

Figure 11.- Comparison of low temperature reacting calculations with equilibrium and combined equilibrium/finite rate chemistry.

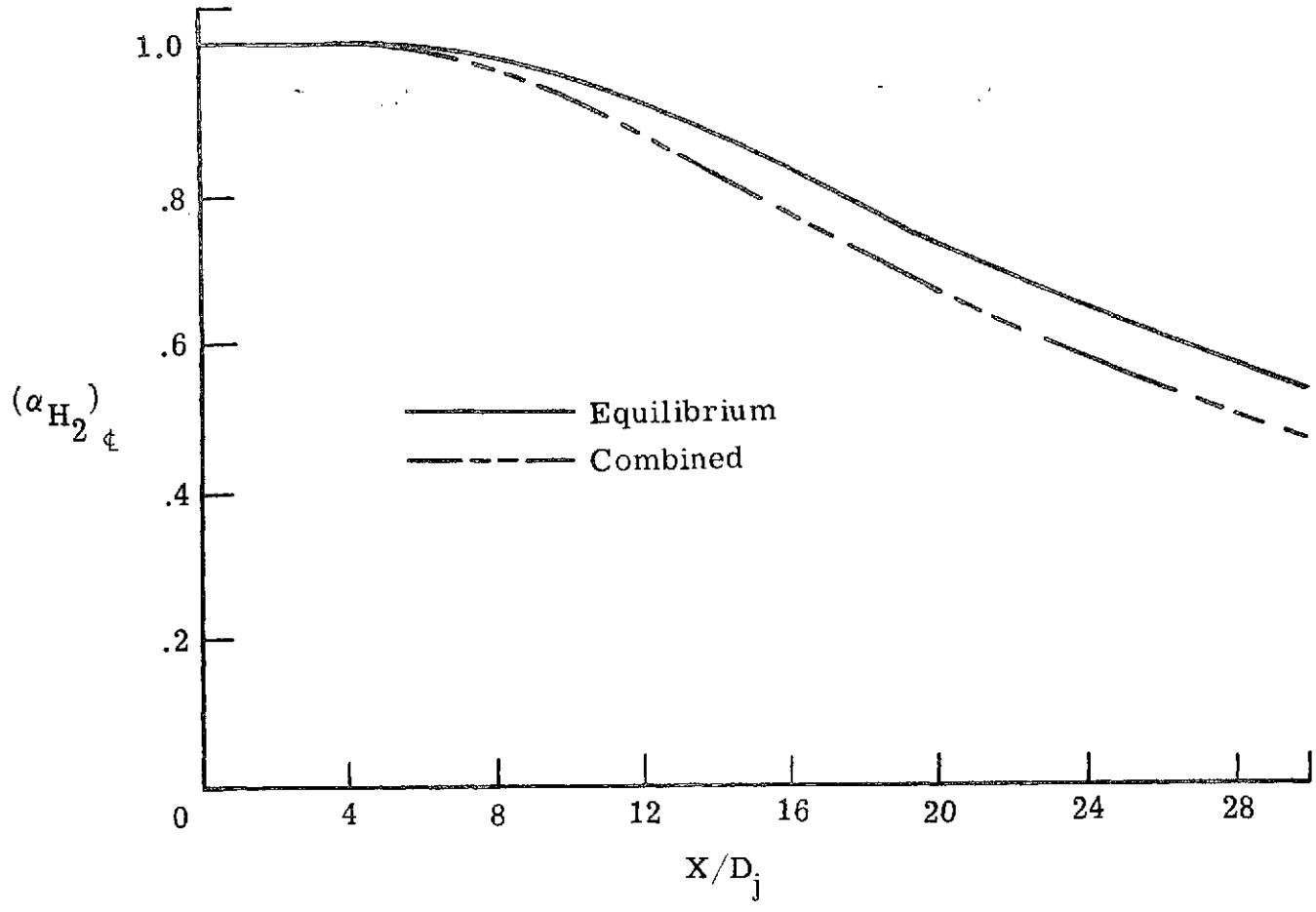

(b) Centerline decay of unreacted hydrogen.

Figure 11.- Continued.

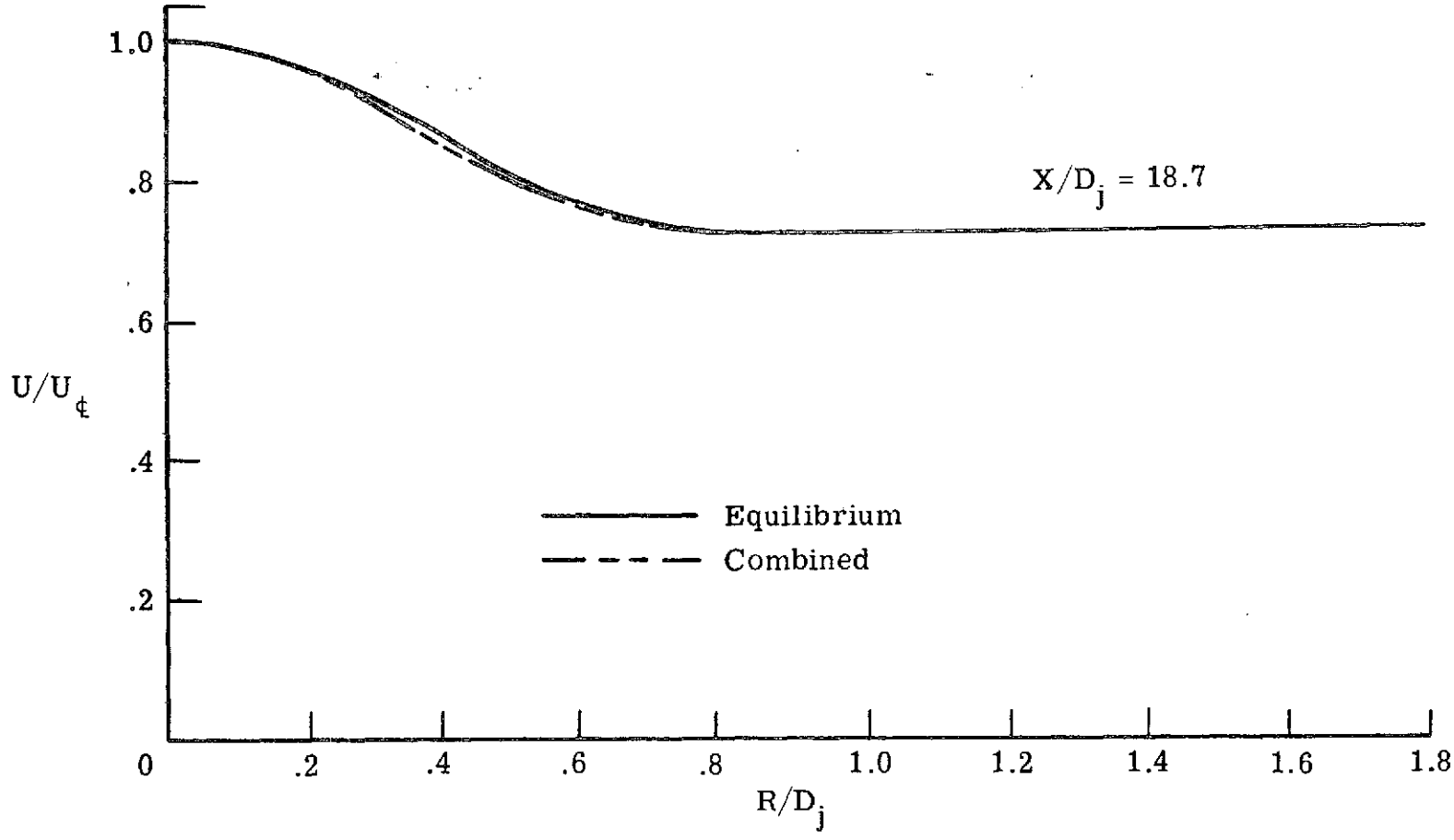

(c) Radial variation of velocity.

Figure 11.- Continued.

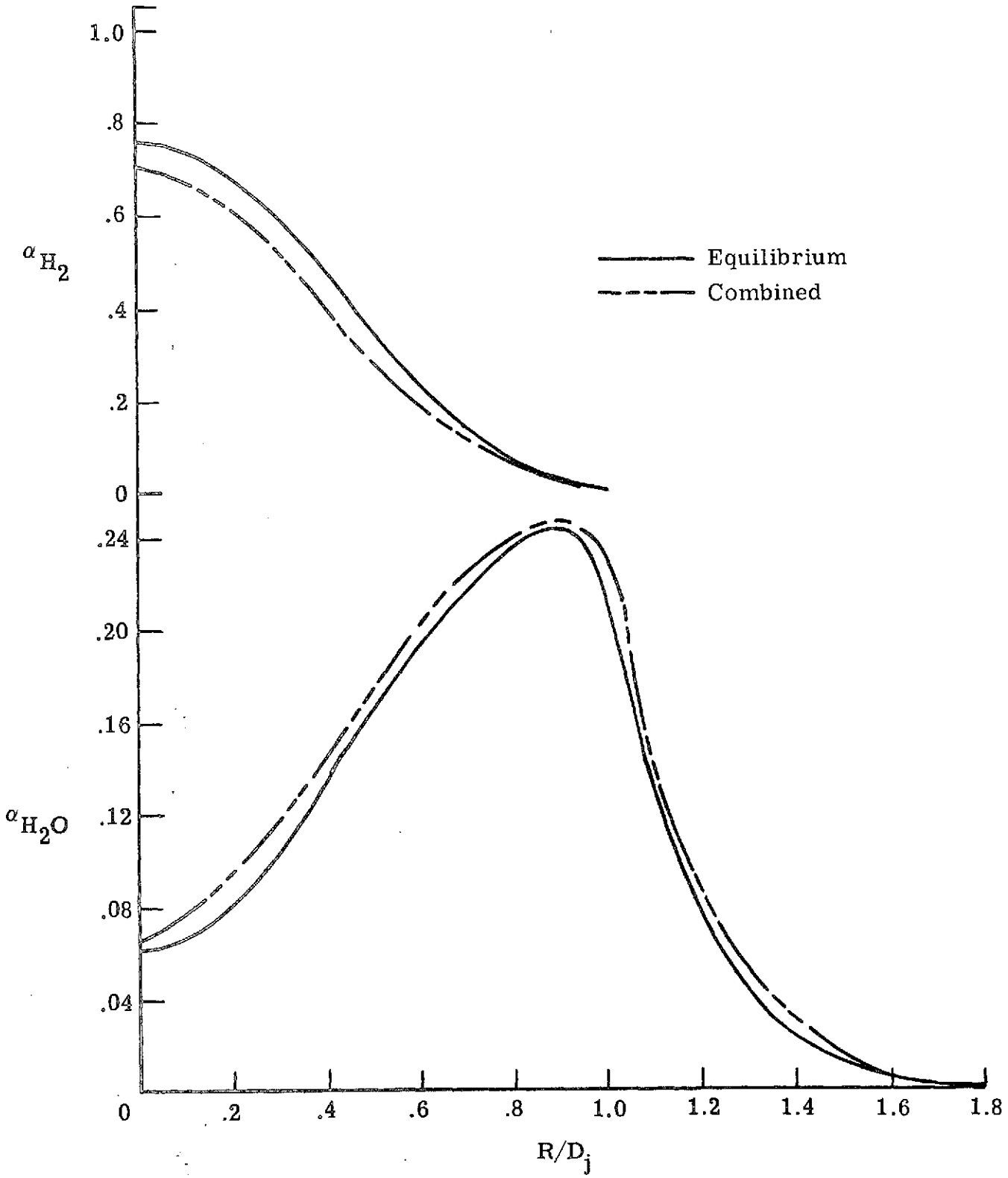

(d) Radial variation of concentration.

Figure 11.- Continued.

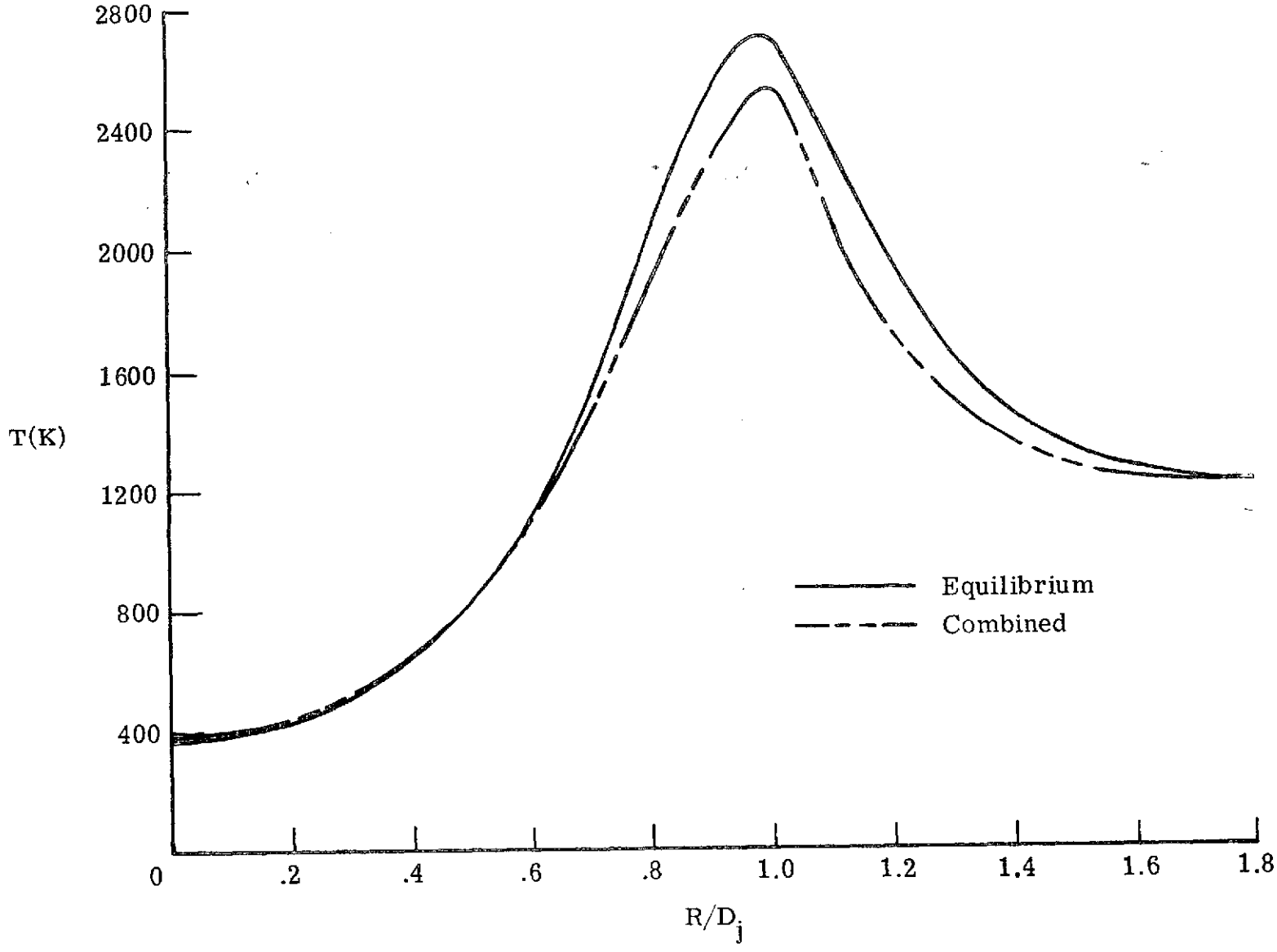

(e) Radial variation of static temperature.

Figure 11.- Concluded.

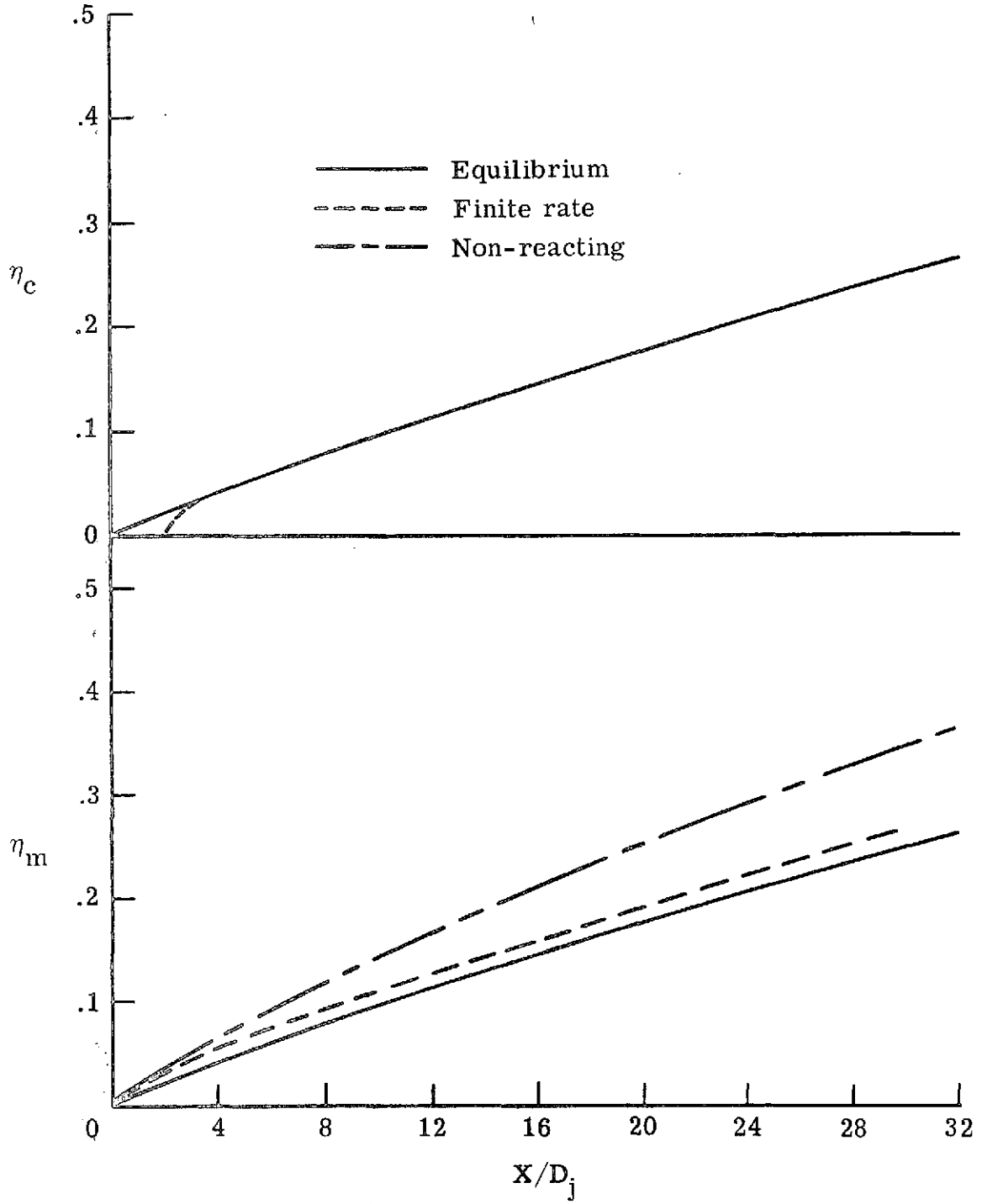

(a) Cases 1 and 2; high temperature.

Figure 12.- Mixing and combustion efficiencies.

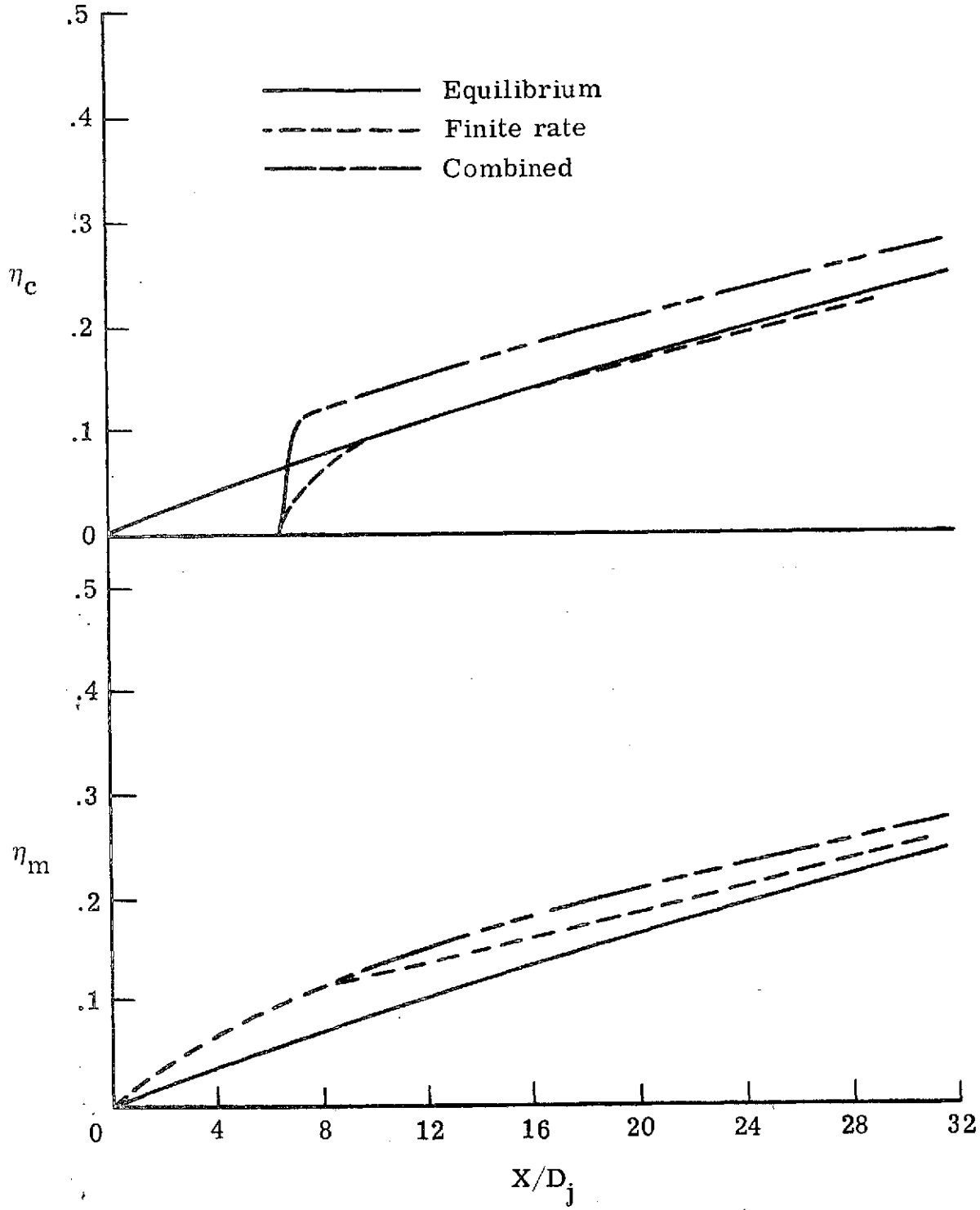

(b) Case 3; low temperature.

Figure 12.- Concluded.

NASA-451

NASA SCIENTIFIC & TECHNICAL INFO.
FACILITY POST OFFICE BOX 8757
BALTIMORE-WASHINGTON INTERNATIONAL
AIRPORT
MARYLAND 21240

30